Geophysical Journal International

Geophys. J. Int.(2011) doi: 10.1111/j.1365-246X.2011.05119.x

New views on earthquake faulting in the Zagros fold-and-thrust belt of Iran

Edwin Nissen,[1] Mohammad Tatar,[2] James A. Jackson[1] and Mark B. Allen[3]

[1]*COMET, Bullard Laboratories, Department of Earth Sciences, University of Cambridge, Madingley Road, Cambridge* CB3 0EZ, *UK. E-mail: ekn20@cam.ac.uk*
[2]*International Institute of Earthquake Engineering and Seismology,* PO Box 19395-3913, *Tehran, Iran*
[3]*Department of Earth Sciences, Durham University, Durham DH1 3LE, UK*

Accepted 2011 June 20. Received 2011 June 20; in original form 2011 March 23

SUMMARY

The Zagros fold-and-thrust belt is amongst the world's most seismically active mountain ranges, and is influential in our understanding of continental collisions. The presence of Hormuz salt at the base of the ∼10 km-thick folded sedimentary cover, together with the general absence of coseismic surface rupturing, have led to an assumption that earthquakes are concentrated within the basement. Here, we reinterpret the seismicity of the Zagros in light of InSAR studies that show some recent earthquakes ruptured the 'Competent Group' of mechanically strong strata in the lower sedimentary cover. Local network data demonstrate that microseismicity occurs within the basement, reaching depths of ∼20 km and in places ∼30 km. Centroid depths of larger ($M_w > 5$) earthquakes are mostly ∼4–14 km, with rare events up to ∼20 km (and ∼28 km along the Oman Line). Within the Simply Folded Belt, most of these events are contained within the Competent Group and are limited to $M_w < 6.1$. However, the M_w 6.7 Ghir and Khurgu earthquakes were too large to have been contained within the Competent Group and probably ruptured both basement and cover. Both are associated with asymmetric anticlines containing rare exposures of Palaeozoic strata, features that may be symptomatic of places where larger ($M_w > 6.5$) earthquakes occur. Earthquakes within the Competent Group can account for much of the overall shortening at this level, but the seismic strain rate in the basement is much lower. It is unclear whether the basement deforms by aseismic creep or folding beneath the SFB or by ductile shortening beneath the High Zagros or Iranian Plateau.

Key words: Earthquake source observations; Seismicity and tectonics; Continental tectonics: compressional; Folds and folding; Asia.

1 INTRODUCTION

Almost 1500 km in length and up to ∼300 km wide, the Zagros mountains of south-western Iran (Fig. 1) are a major structural element of the Alpine–Himalayan belt and one of most rapidly deforming and seismically active fold-and-thrust belts anywhere in the world. The range accommodates around one-third of the total rate of convergence across the Arabia–Eurasia continental collision (Vernant *et al.* 2004), and its instrumental record of high-quality earthquake mechanisms and depths—comprising more than 200 published focal mechanisms and ∼100 independently modelled centroid depths—is unparalleled for a mountain belt of this size.

The Zagros contains a sedimentary cover that spans the entire Phanerozoic and is up to 10–15 km thick (e.g. O'Brien 1957; James & Wynd 1965; Stöcklin 1968; Falcon 1969; Colman-Sadd 1978). With a mixture of strong platform carbonates and weaker evaporites, marls and shales, the stratigraphy has long been known to exert an important influence on the style of deformation. Because of this, and driven also by interest in its vast petroleum reserves, the Zagros has proved a popular testing ground for competing models of fold-and-thrust deformation. However, most of these structural studies are based on observations of surface geology alone, as little seismic reflection or refraction data is available.

The instrumental earthquake record offers a window into the subsurface mechanics of the range, and has also been the focus of several previous studies (e.g. Jackson & Fitch 1981; Berberian 1995; Talebian & Jackson 2004). Partly because of the very rare (Walker *et al.* 2005) and usually absent indications of coseismic ruptures at the surface, these earlier studies concluded that the larger earthquakes in the Zagros involve faulting mostly within the basement. However, more recent geodetic studies, which use radar interferometry (InSAR) to determine the depth extents of coseismic faulting, have revealed that moderate-sized earthquakes (up to $M_w \sim 6$) also occur within the sedimentary cover, rupturing between depths of ∼4 and ∼9 km (Nissen *et al.* 2007, 2010; Roustaei *et al.* 2010). These new results also confirm the existence of active S-dipping reverse faults, in addition to the N-dipping faults expected for a fold-and-thrust belt in which many surface structures verge to the south. A

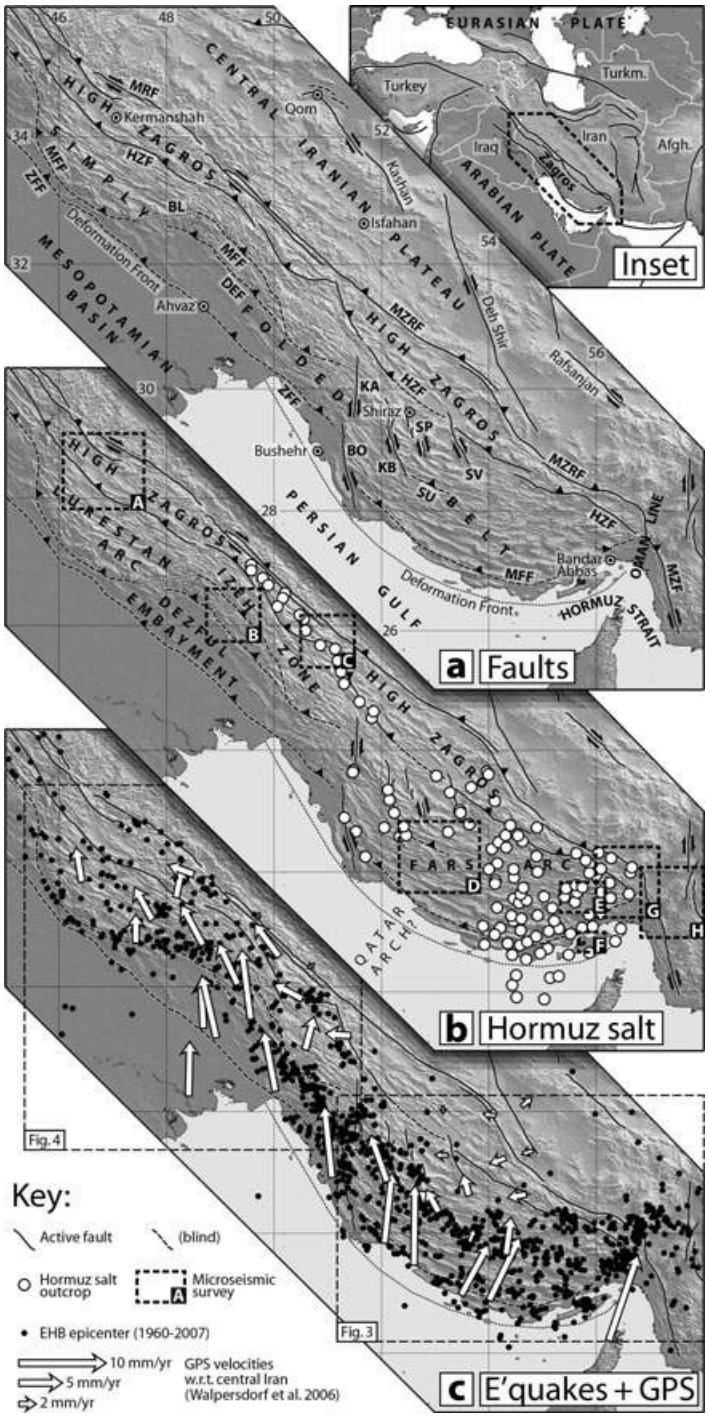

Figure 1. (Inset) Regional tectonic map, with dotted line outlining the location of the main figure. (Main Figure) Topographic map of the Zagros, illuminated from the NE. (a) Major active faults (black lines, dashed if blind). BO, Borazjan Fault; DEF, Dezful Embayment Fault; HZF, High Zagros Fault; KZ, Kazerun Fault; KB, Kareh Bas Fault; MFF, Mountain Front Fault; MRF, Main Recent Fault; MZRF, Main Zagros Reverse Fault; SV, Sarvestan Fault; SP, Sabz Pushan Fault; SU, Surmeh Fault; ZFF, Zagros Foredeep Fault. Dotted lines show other potential major faults, including BL, the Balarud Line. (b) Subdivisions of the Simply Folded Belt, with the distribution of Precambrian–Cambrian Hormuz salt outcrops (white circles) and the areas of local seismic surveys (dashed rectangles) at (A) Kermanshah, (B) Masjed Soleyman, (C) Borujen, (D) Ghir, (E) Fin, (F) Qeshm, (G) Khurgu and (H) Minab. (c) Black dots are epicentres from the updated EHB catalogue of 1960–2007 (Engdahl *et al.* 1998). White arrows are campaign GPS velocities relative to central Iran; these have a precision of $\sim$1 mm yr^{-1} in the Fars Arc and 2 mm yr^{-1} in the NW Zagros (Walpersdorf *et al.* 2006).

peculiar result of these studies was that well-constrained, locally recorded aftershocks of these earthquakes occurred in the basement at depths of $\sim$10–20 km, and were thus vertically separated from the mainshock faulting in the cover.

The aim of this paper is to reinterpret the earthquake record in the light of these recent developments, drawing on observations from eight local microseismic surveys as well as source parameters for the large number of teleseismically recorded earthquakes. We use

patterns contained in these data to address a series of issues, including (1) the relative importance of faulting in the basement versus the cover; (2) links between blind reverse faults and surface folding; (3) the role of detachments at the base of and within the sedimentary cover; (4) possible triggering mechanisms for basement aftershocks following rupture of the lower sedimentary cover and (5) the role of aseismic deformation in accommodating range shortening.

We begin with brief descriptions of the overall tectonic setting of the Zagros and the previous work on its stratigraphy and structure (Section 2). We then discuss results from local networks of seismometers installed in eight different parts of the range (Section 3), followed by a synthesis of well-determined source parameters of teleseismically recorded earthquakes (Section 4). Finally, we draw together these different results to make a series of new observations about the active deformation of the Zagros (Section 5).

2 BACKGROUND

2.1 Tectonic setting

The Zagros mountains represent the deformed north-eastern edge of the Arabian Plate (Inset, Fig. 1). This area existed as a passive continental margin for most of the Phanerozoic, punctuated by periods of extension in the late Palaeozoic and Cretaceous (e.g. Stoneley 1990; Husseini 1992). Following subduction of the Neo-tethys Ocean beneath Iran during the Mesozoic and early Cenozoic, the NE Arabian margin collided with the central Iranian continental block. Estimates of the onset of continental collision range from the late Eocene (e.g. Hessami *et al.* 2001b; Allen & Armstrong 2008) to the mid-late Miocene (e.g. Stoneley 1981; McQuarrie *et al.* 2003), and it may not have been synchronous along the length of the range, possibly starting earlier in the NW than in the SE (Gavillot *et al.* 2010). Present-day rates of N–S shortening (measured with GPS) also vary along the length of the range, from a maximum of $\sim$9 mm yr^{-1} in the SE to $\sim$4 mm yr^{-1} in the NW (Vernant *et al.* 2004; Walpersdorf *et al.* 2006). Despite the high level of seismicity, summed earthquake moments can only account for a small proportion of the total convergence (Jackson & McKenzie 1988; Masson *et al.* 2005).

To the SW of the Zagros mountains, the Mesopotamian basin (in the NW) and the Persian Gulf (in the SE) are foreland basins on undeformed parts of Arabian Plate, lying at or near sea level with estimated crustal thicknesses of 40–50 km (e.g. Al-Amri & Gharib 2000; Al-Damegh *et al.* 2005; Gök *et al.* 2008). The deformation front on this side of the range follows an approximately linear south-easterly trend across the Mesopotamian basin and NW Persian Gulf, but then curves round to trend E and then NE in the central Gulf and the Strait of Hormuz (Fig. 1a). As a result, N–S shortening is oblique to the range in the NW (where there is a significant right-lateral component of motion) but perpendicular to it in the SE. In the far SE, northward indentation by the Arabian Plate forms a syntaxis known as the Oman Line (e.g. Kadinsky-Cade & Barazangi 1982), accompanied by an abrupt change in structural orientation along the N–S Minab-Zenden fault zone (Fig. 1a), which connects with the Makran subduction zone in SE Iran.

To the NE of the Zagros, the Central Iranian Plateau averages $\sim$2 km in elevation. The suture between deformed Arabian margin sediments and volcanic and metamorphic rocks of central Iran roughly follows the Main Zagros Reverse Fault (MZRF; sometimes termed the Main Zagros Thrust), an important basement structure which marks the NE boundary of the range (e.g. Stöcklin 1974; Falcon 1974; Berberian 1995; Regard *et al.* 2004). Immediately NE of the MZRF, the Sanandaj–Sirjan zone contains metamorphosed rocks thought to belong to the Central Iranian continental block, although this area is sometimes included within the Zagros itself (e.g. Alavi 2007). Further NE (but still within the Central Iranian Plateau), the Urumieh–Dokhtar magmatic arc contains Andean-type calc-alkaline volcanics related to subduction of the Neo-Tethys. Crustal thicknesses determined by seismic receiver functions are up to 55–70 km in the Sanandaj–Sirjan zone, decreasing north-eastwards to 40–50 km in the Urumieh–Dokhtar magmatic arc (Rham 2009; Paul *et al.* 2010).

The Zagros range can be divided into two zones that are distinct in their topography, geomorphology, exposed stratigraphy and seismicity. The $\sim$100 km wide north-eastern zone, called the High Zagros (Fig. 1a), averages 1.5–2 km in elevation (with numerous peaks over 4000 m) and exposes stratigraphic levels in the Mesozoic and Palaeozoic (discussed in more detail in Section 2.2). The 100–200 km wide south-western zone, called the Simply Folded Belt (SFB), rises from sea level in the SW to $\sim$1.5 km in the NE (Fig. 1a) and exposes Palaeozoic strata only rarely (except for the Hormuz salt plugs). The SFB is dominated by the large, open, linear folds for which the range is famous (e.g. Oberlander 1965; Falcon 1969; Colman-Sadd 1978; Ramsey *et al.* 2008). The SFB can be further subdivided along-strike into two lobate salients containing high relief (the Lurestan Arc and Fars Arc) separated by a recess with relatively low-lying topography (the Dezful Embayment; Fig. 1b). A second recess in northern Iraq (the Kirkuk Embayment) is also part of the Zagros, but with relatively few focal mechanisms and no local network data we do not consider it in our study.

The regionally averaged topographic slope across the SFB is very low for an intracontinental mountain belt, typically $<1^\circ$ and only approaching 2° across the narrow ($\sim$100 km-wide) strip between the Dezful Embayment and the HZF (McQuarrie 2004). In detail, however, this regional slope rarely corresponds to a simple, planar surface, but is usually stepped (Mouthereau *et al.* 2007). Moho depths inferred from receiver functions are typically $\sim$45 km under the Zagros, although the extent to which crustal thicknesses vary across the mountain belt is debated. Rham (2009) shows Moho depths increasing steadily from $\sim$40 km at the south-western edge of the SFB to $\sim$55 km at the MZRF, whereas Paul *et al.* (2010) support a uniform Moho depth of 40–45 km across the whole width of the Zagros, only becoming deeper close to the MZRF.

2.2 Stratigraphy

The Zagros contains a thick sedimentary cover which records near-continuous deposition since the late Precambrian (e.g. O'Brien 1957; James & Wynd 1965; Stöcklin 1968; Falcon 1969; Colman-Sadd 1978). Many aspects of the stratigraphy are maintained along the full length of the range, although there are also important changes along strike. In this section, we summarize the most important observations in the context of this study; more detailed descriptions of the stratigraphy are provided elsewhere (e.g. Alavi 2004). Generalized stratigraphic columns for the Lurestan Arc, Dezful Embayment and SE Fars Arc [from Casciello *et al.* (2009), Sherkati *et al.* (2005) and Molinaro *et al.* (2005), respectively] are shown in Fig. 2.

Given the scarcity of high-quality seismic reflection or refraction data, there are few direct constraints on the total sedimentary thickness. Perhaps the most reliable estimates come from summing individual stratigraphic units, but rely on assumptions made about

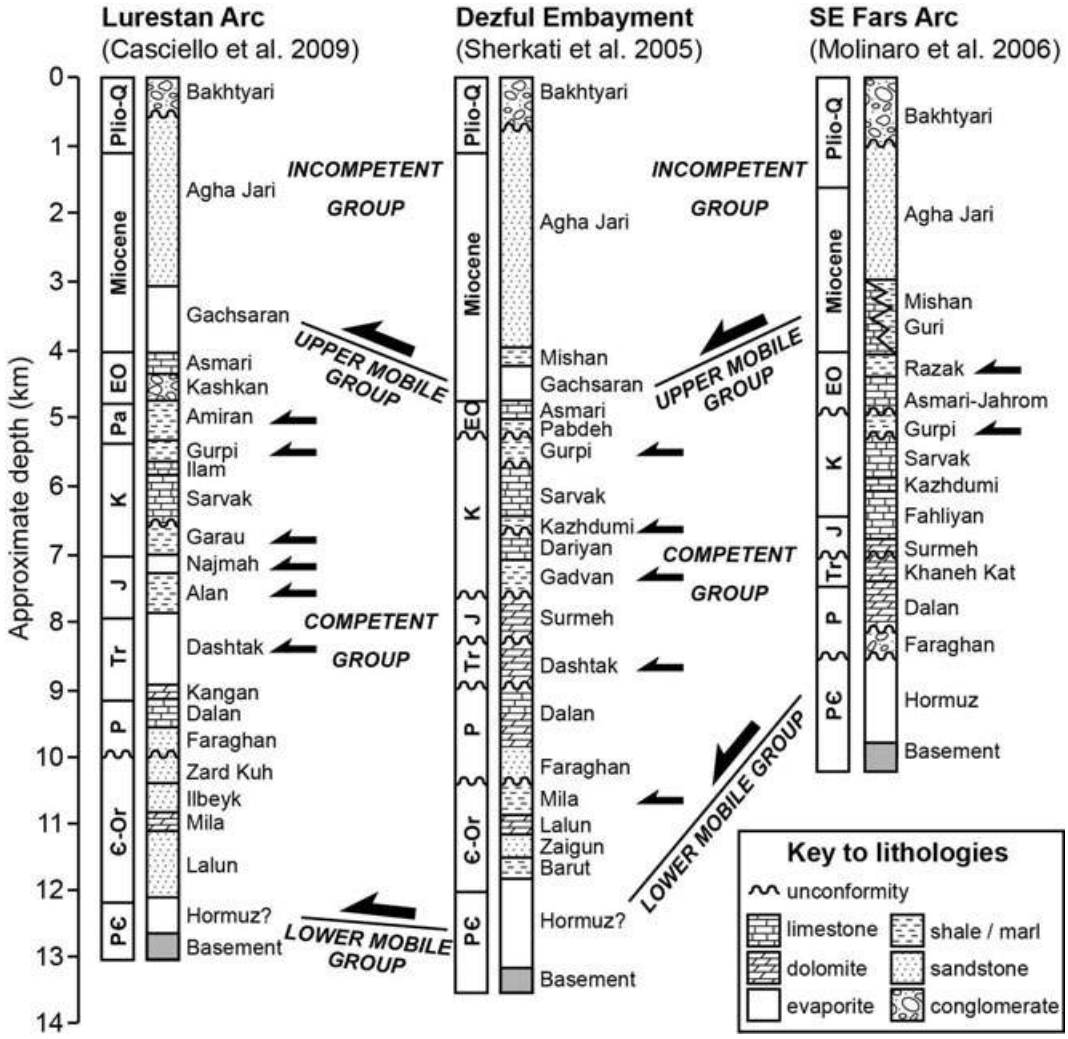

Figure 2. Generalized stratigraphic columns with approximate depths for the Lurestan Arc (Casciello *et al.* 2009), Dezful Embayment (Sherkati *et al.* 2005) and SE Fars Arc (Molinaro *et al.* 2005). Ages are abbreviated as follows: Plio-Q, Pliocene–Quaternary; EO, Eocene–Oligocene; Pa, Palaeocene; K, Cretaceous; J, Jurassic; Tr, Triassic; P, Permian; ∈-Or, Cambrian–Ordovician; P∈, Precambrian. The mechanical divisions of O'Brien (1957) are shown in italics, with large arrows designating the most important weak horizons. More minor weak layers are marked by smaller arrows.

the lateral continuity of each layer. This strategy yields thicknesses of ∼14 km in the north–west SFB, ∼12 km in the central Fars Arc and ∼10 km in the far south-eastern SFB (e.g. Colman-Sadd 1978; Molinaro *et al.* 2005; Sherkati *et al.* 2005; Casciello *et al.* 2009), amounts that decrease north-eastwards into the High Zagros where much of the younger cover has been removed by erosion. Modelling aeromagnetic data (Kugler 1973; Morris 1977) yields a wider range of basement depths, between 4 km and 18 km, but these estimates are based on long-wavelength signals and are not well-constrained locally (Talebian 2003). In the central Fars Arc, an analysis of locally recorded earthquake arrival times indicates a step-wise increase in seismic velocities at ∼11 km, interpreted by Hatzfeld *et al.* (2003) to represent the top of the basement. However, not all local earthquake surveys in the Zagros reveal such a clear jump in seismic velocities (see Section 3), placing doubt on whether the basement-cover interface can reliably be detected in this way.

There are no basement outcrops in the Zagros, and the oldest exposed unit is the late Precambrian–Cambrian Hormuz salt. Seismic lines in the Persian Gulf suggest that in places even older sediments underlie these evaporites (Jahani *et al.* 2009)—though this may not be the case across the whole range—and blocks of igneous, metamorphic and sedimentary rock entrained within the salt provide rare specimens of this underlying material (Kent 1979). The Hormuz salt itself never appears as a complete stratigraphic sequence but is instead brought to the surface in scattered diapirs (e.g. O'Brien 1957; Kent 1979), which are observed in three main areas: (i) the eastern Fars Arc, (ii) along the Kazerun, Borazjan and Sarvestan strike-slip faults in the western Fars Arc and (iii) in the High Zagros NE of the Dezful Embayment (Fig. 1b). Stratigraphic relations indicate that the diapirs have been active since the Palaeozoic, and thus predate the onset of continental collision (Jahani *et al.* 2007). The original thickness of Hormuz salt is believed to be at least 1 km on the basis of the size of the largest blocks of country rock entrained within the diapirs (Kent 1979), but it is not clear how much salt remains in place stratigraphically at depth.

The Hormuz salt is often assumed to be completely absent from the Dezful Embayment and the Lurestan Arc. Bahroudi & Koyi (2003) suggest that the division of the range into salients and recesses is governed by the presence or absence of Hormuz salt in these areas, although the low-angle topographic taper observed in Dezful and Lurestan hints at the continued presence of a deep detachment horizon, consisting of Hormuz salt or something else

(McQuarrie 2004; Sherkati & Letouzey 2004; Carruba *et al.* 2006). The apparent absence of Precambrian salt from central Fars Arc is also puzzling, but may be related to a NE-trending structural high (the 'Qatar Arch', Fig. 1b) which is visible in isopach maps (Koop & Stoneley 1982) and may have controlled deposition during the late Proterozoic (e.g. Murris 1980; Bahroudi & Koyi 2003; Jahani *et al.* 2009).

Palaeozoic through to Oligocene strata are dominated by massive platform carbonates and coarse clastics, which total ∼5 km in thickness and are collectively termed the 'Competent Group' (O'Brien 1957). Palaeozoic units are mostly known from the High Zagros with only very rare exposures in the SFB. Mesozoic and Palaeocene rocks are much more widespread at the surface and are exposed in both the High Zagros and SFB (though notably not the Dezful Embayment). They also contain several potential décollement horizons, in marl, shale and evaporite layers such as the Triassic Dashtak evaporites, Cretaceous Gurpi and Kazhdumi Formations, and Palaeocene-Eocene Pabdeh marls [e.g. Sherkati & Letouzey (2004); Sepehr *et al.* (2006); Fig. 2]. The Competent Group is capped by the Oligocene–Lower Miocene Asmari limestone, which is also one of the main petroleum reservoirs in the region.

Miocene strata consist of Gachsaran evaporites in the NW and Mishan marls in the SE (Fig. 2). Collectively termed the Upper Mobile Group (O'Brien 1957), these mechanically weak units are the youngest marine sediments in the Zagros and often act as the cap to regional petroleum reserves. Overlying these are up to 4 km of foreland basin infill, comprising Agha Jari sandstones overlain unconformably by coarse Bakhtyari conglomerates. Derived from the initial uplift and erosion of the range, the Bakhtyari conglomerates have long been considered key to understanding the timing of continental collision. Recent bio- and magnetostratigraphic work suggests that their age varies considerably, being Plio-Pleistocene in the active foreland, early Miocene in the northern Fars Arc, and possibly as old as the Oligocene in parts of the High Zagros, reflecting propagation of the deformation front and foreland basin towards the SW (Homke *et al.* 2004; Fakhari *et al.* 2008; Khadivi *et al.* 2010).

2.3 Structure, faulting and folding

2.3.1 High Zagros

There is a clear structural distinction between the High Zagros and the SFB (Fig. 1a). The High Zagros contains imbricated slices of Mesozoic and Palaeozoic sediments as well as ophiolites that were emplaced onto Arabian passive margin during the Late Cretaceous (Stoneley 1990). Its NW-striking thrust and reverse faults are well exposed at the surface, the most important ones being the MZRF and the High Zagros Fault (HZF; Figs 1a, 3, and 4). The MZRF is generally considered to follow the suture between Arabian rocks and those of central Iran [though see Alavi (2007)], but GPS measurements suggest that it is no longer active except in the NW where it is coincident with the right-lateral Main Recent Fault (e.g. Walpersdorf *et al.* 2006). The HZF constitutes the boundary with the SFB, and was the location of the only known case of reverse-faulting coseismic surface rupture in the Zagros, during the 1990 November 6 Furg earthquake (M_w6.5) in the far SE of the range [Walker *et al.* (2005); Fig. 3c]. The region NE of Shiraz is at odds with this general description; the HZF is blind in this area, which instead contains gentle folding more commonly associated with the SFB (Fig. 3).

The north-western part of the High Zagros also contains an important NW–SE-trending right-lateral strike-slip fault known as the Main Recent Fault (MRF; Figs 1a and 4). The MRF roughly follows the Arabia–Iran suture from ∼45°E (close to the Turkey–Iran border) to ∼51°E, possibly reactivating high-angle reverse faults (Authemayou *et al.* 2006), and is thought to accommodate much of the right-lateral component of Arabia–Iran motion in the north-western Zagros (e.g. Talebian & Jackson 2002). Estimates of its active slip-rate range from 2–3 mm yr^{-1} from GPS (Vernant *et al.* 2004; Walpersdorf *et al.* 2006) to 3.5–12.5 mm yr^{-1} from displaced Late Quaternary landforms (Authemayou *et al.* 2009), while drainage patterns indicate a cumulative offset of 50–70 km (Talebian & Jackson 2002).

2.3.2 Simply Folded Belt

The structure of the SFB is very different from that of the High Zagros. Here, the only major faults to cut the surface are a series of roughly N–S, right-lateral faults in the western Fars Arc—the Kazerun, Borazjan, Karebas, Sabz Pushan and Sarvestan faults (Figs 1a and 3). GPS measurements suggest these faults have a combined right-lateral slip-rate of ∼6 mm yr^{-1} (Walpersdorf *et al.* 2006; Tavakoli *et al.* 2008). About 4 mm yr^{-1} of this is accommodated by the Kazerun fault alone, in agreement with dating of offset Late Quaternary structures (Authemayou *et al.* 2009).

These strike-slip faults have N- or NNW-directed earthquake slip vectors, oblique to the NE-oriented slip vectors of neighbouring thrust events, and they cannot therefore be considered transform faults. Authemayou *et al.* (2006) suggest that they link northwestwards with the Main Recent Fault, essentially comprising the horsetail termination of this latter strike-slip fault. Noting that many of them are absorbed at their southern ends by major blind thrusts such as the Surmeh Fault (Fig. 3), Hessami *et al.* (2001a) and Talebian & Jackson (2004) suggest that the faults rotate anticlockwise about vertical axes. However, palaeomagnetic data are at present too limited to confirm or exclude such rotation (Aubourg *et al.* 2008). Whether or not these faults rotate, their NE–SE *T*-axes achieve the along-strike extension required by a transition from oblique convergence in the NW Zagros and range-perpendicular shortening in the SE.

The seismicity of the SFB is dominated by blind thrust faulting, which is seldom associated with surface rupturing (Walker *et al.* 2005). Shortening at the surface is instead accommodated by parallel trains of anticlines and synclines. Most anticlines are expressed in resistant units such as the Asmari limestone, giving rise to the characteristic 'whaleback' mountains for which the Zagros is famous. Folding is generally symmetric, with typical half-wavelengths of ∼10 km and amplitudes of ∼4 km. On closer inspection, however, folding comes in a wide variety of styles and the name 'SFB' is somewhat misleading.

The mechanism of folding within the SFB is the focus of a large body of work, much of it investigating the influence of buried faulting and/or lateral variations in the stratigraphy. Early studies suggested that folding was caused by buckling of sediments ('detachment folding') along decollements within the sedimentary cover, most notably the Late Proterozoic Hormuz and Miocene Gachsaran evaporites (e.g. Stöcklin 1968; Falcon 1969; Colman-Sadd 1978; Jackson 1980). Weak horizons at higher stratigraphic levels can also play an important role; where they are thick enough (greater than ∼1 km), these can even promote disharmonic folding of the layers below and above (Sherkati & Letouzey 2004; Sepehr *et al.* 2006; Casciello *et al.* 2009). In some of these models, the

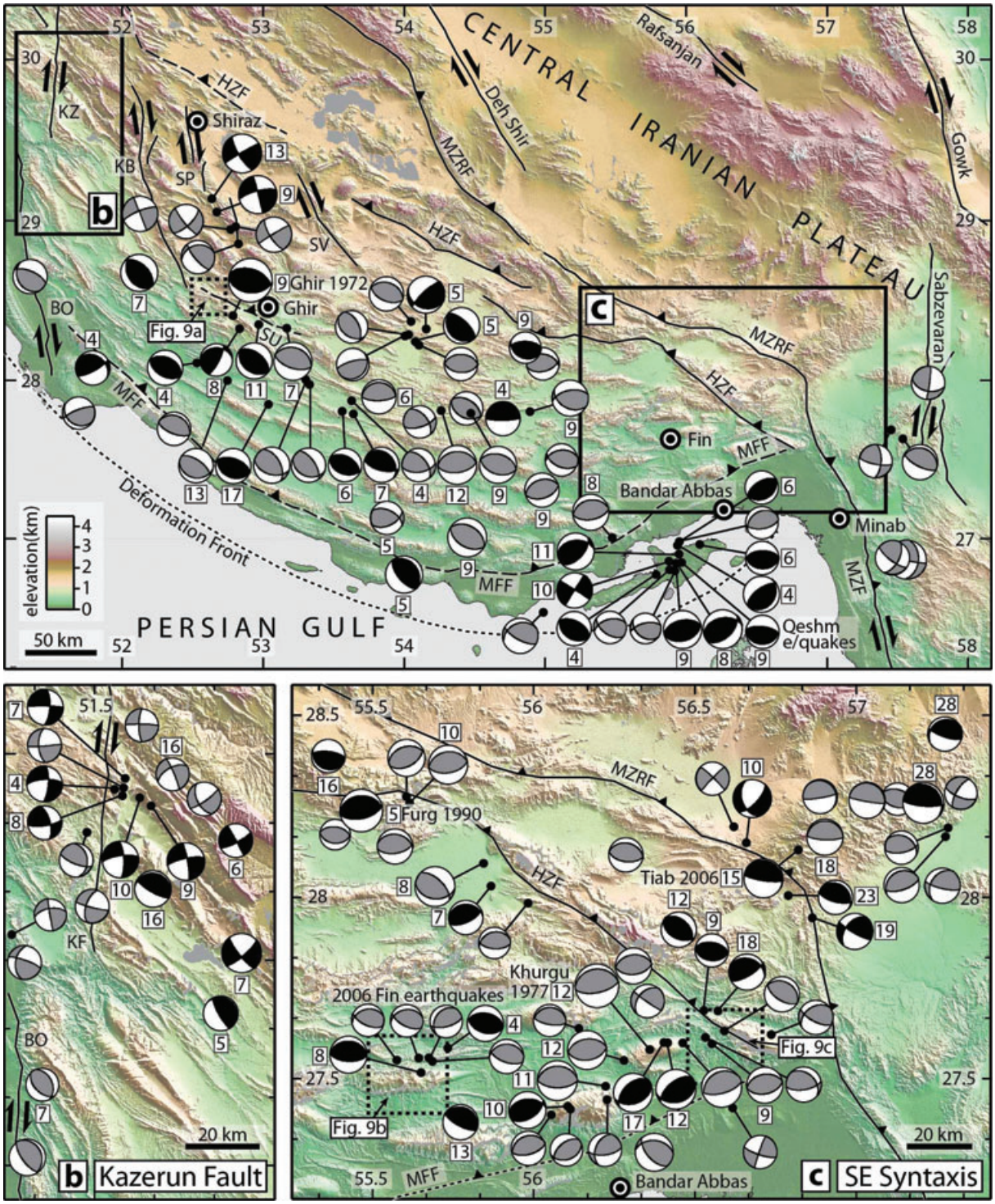

Figure 3. Topography, major active faults and earthquake focal mechanisms in the south-eastern Zagros, including insets showing (a) the Kazerun Line and (b) the south-eastern syntaxis. Black mechanisms have been determined from full *P* and *SH* body-wave modelling, and are shown with centroid depths in kilometres. Grey mechanisms are from first motions or the Global CMT catalogue; some have centroid depths (in kilometre) independently constrained from *P* and/or *S* waves or InSAR. Full details of all these earthquake source parameters are provided in the supplementary material (Table S1). Dotted rectangles outline the areas viewed in perspective in Fig. 7.

sedimentary cover is often assumed to be completely aseismic, with faulting restricted to the crystalline basement (e.g. Mouthereau *et al.* 2007). Other structural interpretations link each surface anticline to a blind thrust buried within the cover, which controls its growth through fault propagation or fault bending ('forced folding'). In these models, the blind thrusts are usually N-dipping and nucleate either within the lower part of the sedimentary cover (McQuarrie 2004; Alavi 2007) or within the underlying basement, breaking through the Hormuz salt and passing upwards into the sediments (Berberian 1995).

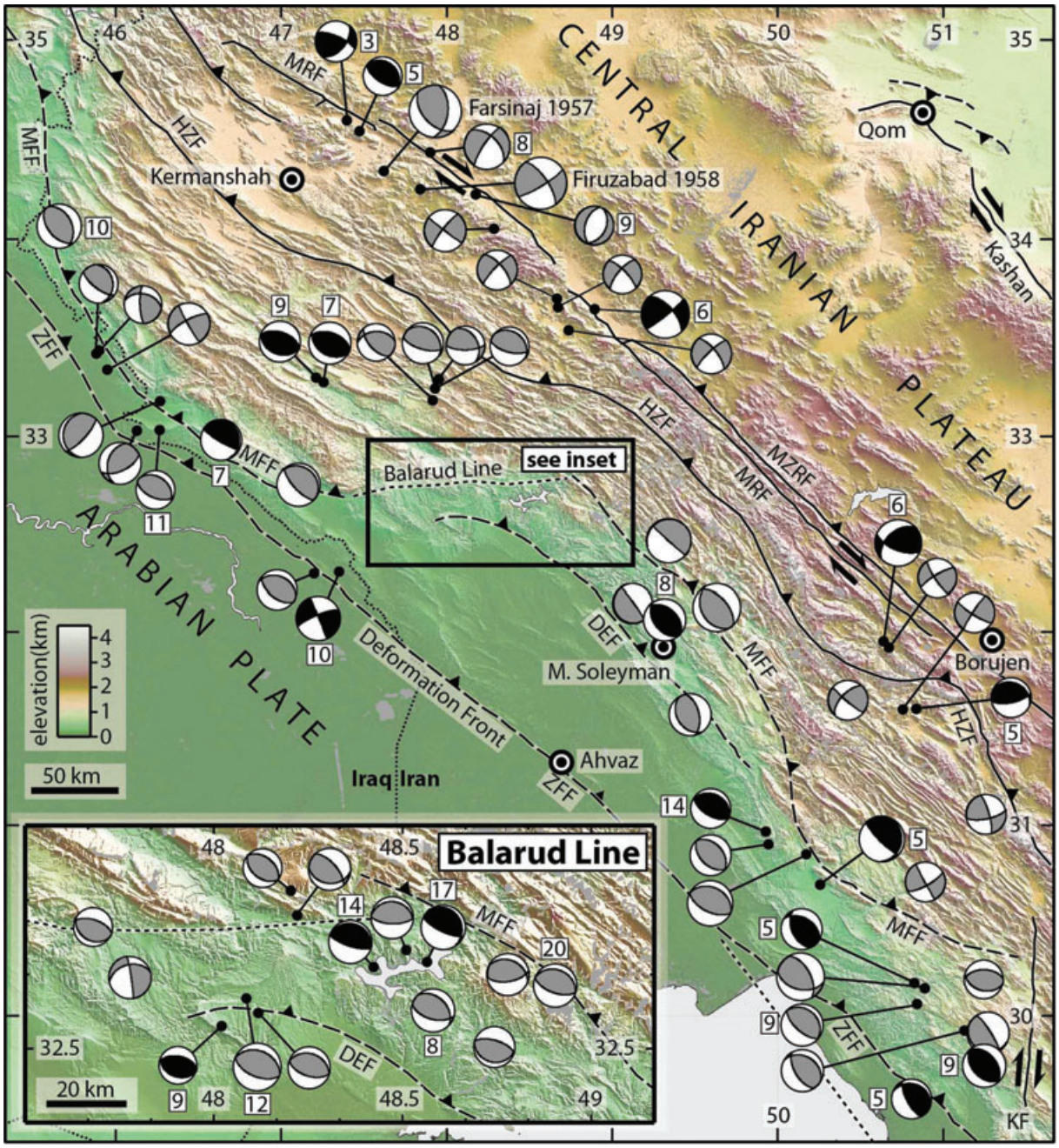

Figure 4. Topography, major active faults and earthquake focal mechanisms in the north-western Zagros, including an inset showing the Balarud Line. Earthquake mechanisms are as for Fig. 3, with full details provided in the supplementary material (Table S1).

There is a significant change in the stratigraphical level (and sometimes elevation) across certain folds in the SFB, which Berberian (1995) linked to major, N-dipping basement faults, termed 'master blind thrusts' (Fig. 1a). The most important of these is the Mountain Front Fault (MFF), which marks the south-western limit of the surface exposure of Asmari limestone. The MFF has a throw of ∼2–4 km in the Lurestan and Fars Arcs (Blanc *et al.* 2003; Molinaro *et al.* 2005; Emami *et al.* 2010) and up to ∼6 km in the Dezful Embayment (Berberian 1995; Sherkati *et al.* 2006). A second major basement thrust, the Zagros Foredeep Fault (ZFF), separates folds of Agha Jari and Bakhtyari rocks from the Quaternary alluvium of the Mesopotamian Basin and northern Persian Gulf coast and accommodates a throw of up to ∼3 km in the Dezful Embayment (Berberian 1995). However, in parts of the Lurestan and Fars Arcs the MFF and ZFF lie within a few kilometres of one another and in these areas they may actually represent a single structural step, rather than two distinct steps. There is also no evidence to suggest that these basement faults were colinear along strike when formed; for instance, Berberian (1995)'s MFF appears to be offset by ∼140 km along the Kazerun Fault, many times the actual cumulative displacement on this structure (Authemayou *et al.* 2006).

Shorter blind basement thrusts have been inferred in other parts of the range (e.g. Berberian 1995; Leturmy *et al.* 2010). These include the Dezful Embayment Fault (DEF), which marks a stratigraphic step of ∼1–3 km in the central Dezful Embayment (Berberian 1995;

Blanc *et al.* 2003). The Surmeh fault forms the southern termination of the Kareh Bas strike-slip fault in the western Fars Arc, and brings lower Palaeozoic rocks to the surface in what is their only exposure in the entire SFB. These faults are all plotted on Figs 1(a), 3 and 4.

Not all published studies confine themselves to the two end-member structural styles of detachment folding and forced folding and some involve a combination of the two (e.g. Hessami *et al.* 2001b; Blanc *et al.* 2003; Sepehr *et al.* 2006). Other work suggests that the folding mechanism may have changed over time, comprising an early thin-skinned stage of detachment folding followed by a thick-skinned stage involving basement faulting and forced folding (Molinaro *et al.* 2005; Sherkati *et al.* 2005). Such two-stage models are derived from an overprinting of fold styles in the far south-eastern SFB, so it is not clear whether they can be extrapolated across the whole range. Whatever the preferred mechanism of folding, balanced cross-sections of the whole SFB give remarkably consistent estimates of 50–80 km for the total shortening of the cover (Blanc *et al.* 2003; McQuarrie 2004; Sherkati *et al.* 2006; Mouthereau *et al.* 2007).

Finally, there is evidence that deformation within the SFB cover has migrated from NE to SW through time. Hessami *et al.* (2001b) associated the onset of tectonic uplift with a suite of unconformities that become progressively younger towards the foreland in the SW. More recently, direct support for this migration has come from the diachronous age of the Bakhtyari conglomerates (e.g. Homke *et al.* 2004; Fakhari *et al.* 2008; Khadivi *et al.* 2010), and also from GPS and geochronological data which suggest that shortening in central Fars is concentrated within ∼100 km of the Persian Gulf coastline (Walpersdorf *et al.* 2006; Oveisi *et al.* 2009). However, shortening across the NW SFB is more evenly distributed (Walpersdorf *et al.* 2006), and growth strata in anticlines of the frontal Lurestan Arc show uplift occurring by ∼8 Ma, since which time the SW limit of deformation has remained fixed (Homke *et al.* 2004).

3 LOCALLY-RECORDED EARTHQUAKES

In this section, we use data from a series of local seismic networks to help characterize the seismogenic thickness and seismic velocities of the Zagros. Included are published results from six previous networks, as well as data from two new networks that are presented here for the first time (Fig. 1b). The published surveys each targeted the epicentral area of a recent moderate-sized earthquake, and consisted of up to 49 seismometers deployed for periods of up to 3 months. These surveys are at Borujen in the central High Zagros (Yamini-Fard *et al.* 2006), Ghir in the western Fars Arc (Hatzfeld *et al.* 2003; Tatar *et al.* 2004), Fin, Qeshm and Khurgu in the SE Fars Arc (Roustaei *et al.* 2010; Nissen *et al.* 2010; Gholamzadeh *et al.* 2009), and Minab in the Zagros-Makran syntaxis (Yamini-Fard *et al.* 2007). The two new surveys, with fewer seismometers but installed for longer periods (>3 years), are at Kermanshah in the NW High Zagros and Masjed Soleyman in the N Dezful Embayment (Fig. 1b).

The instrumentation and processing used in each survey varies in detail, but can be broadly described as follows. Each network contained a combination of short-period, one-component (vertical) seismometers and short-period or broadband three-component seismometers. Initially, the V_p/V_s ratio was calculated by plotting $T_{sj} - T_{si}$ (the *S* arrival time at station *i* minus that at station *j*) versus $T_{pj} - T_{pi}$ (the *P* arrival time at station *i* minus that at station *j*) for all events and all stations. A subset of earthquakes was then chosen, containing the best-recorded events selected according to their azimuthal gap, RMS residual arrival time, and number of separate *S* and *P* phase recordings (the exact criteria for each individual survey are given in Fig. 5). The arrival times of this subset were inverted to determine, simultaneously, improved hypocenters and an enhanced 1-D velocity structure (Kissling 1988). Because the results vary according to the initial velocity model, the inversion was run ∼100 times using randomly perturbed starting models. The final velocity model was calculated by averaging those results which yielded a clear improvement in the arrival time residuals (e.g. Tatar *et al.* 2004).

Model results suggest that *P*-wave velocities in the sedimentary cover are 5.0–5.6 km s^{-1} (Fig. 5). However, only at Masjed Soleyman, Ghir and Minab are there large (∼1 km s^{-1}) increases in V_p at levels that might correspond to the base of the cover. The lack of a widespread, systematic step in V_p across all surveys may indicate that velocities in the uppermost basement remain relatively slow, although adequate resolution may be a problem. It may therefore not generally be possible to estimate the basement-cover interface from such a velocity contrast, in spite of the case made for this at Ghir in the well-resolved study by Hatzfeld *et al.* (2003).

Maps of the resulting earthquake hypocentres, coloured according to depth, are provided in Supplementary Material. In most of the surveys the distribution of microseismicity is diffuse, although there are concentrations along the High Zagros Fault near Kermanshah (Fig. S2). Where it was possible to determine fault-plane solutions, these tend to be consistent with teleseismic focal mechanisms in the same area. In general there are few low-angle thrust faulting mechanisms, except near Masjed Soleyman where teleseismically recorded earthquakes also involve low-angle thrusting (Fig. 4).

In assessing the quality of the locally recorded earthquake locations, we paid particular attention to the estimates of hypocentral depths. These are plotted (together with the best-fit velocity structures) in Fig. 5. For each survey, the subset of best-recorded events with the most robust depths (formal errors less than 2–3 km) are shown in black, with more poorly constrained data shown in grey. The best located earthquakes have both *P* and *S* arrivals at close stations with good azimuthal coverage. Nonetheless, most of these local networks had typical station spacing of ∼10–20 km and are therefore most accurate in determining depths in the range of 10–20 km. Hypocentres are more difficult to determine accurately when their depth is much less than the stations spacing (unless they happen to occur beneath a particular station), so the general lack of well-resolved earthquakes shallower than ∼10 km should not be taken too seriously (Fig. 5). However, hypocentres at depths greater than ∼10 km—and the deeper cut-off to this microseismicity distribution—are generally well-determined.

A common observation from all the surveys is the abundance of earthquakes at depths >10 km. These hypocentral depths are well-resolved, and most of these events must be in the basement. Only at Borujen in the High Zagros are well-resolved earthquakes also common at depths of <5 km (Fig. 5c), probably due to the relatively close station spacing (∼5–10 km) in this particular network. This is also an area containing abundant surface exposures of Lower Palaeozoic rocks, and many of these shallow events may still be occurring within the basement. The deeper cut-off in microseismicity varies between the different surveys but is always ≥20 km. Earthquakes deeper than 20 km are rare except at Fin, where there are a large number of events at 20–30 km (Fig. 5e), and at Minab on the Oman Line (Fig. 1b), where well-resolved hypocentral depths reach 35–40 km (Figs 5a and h).

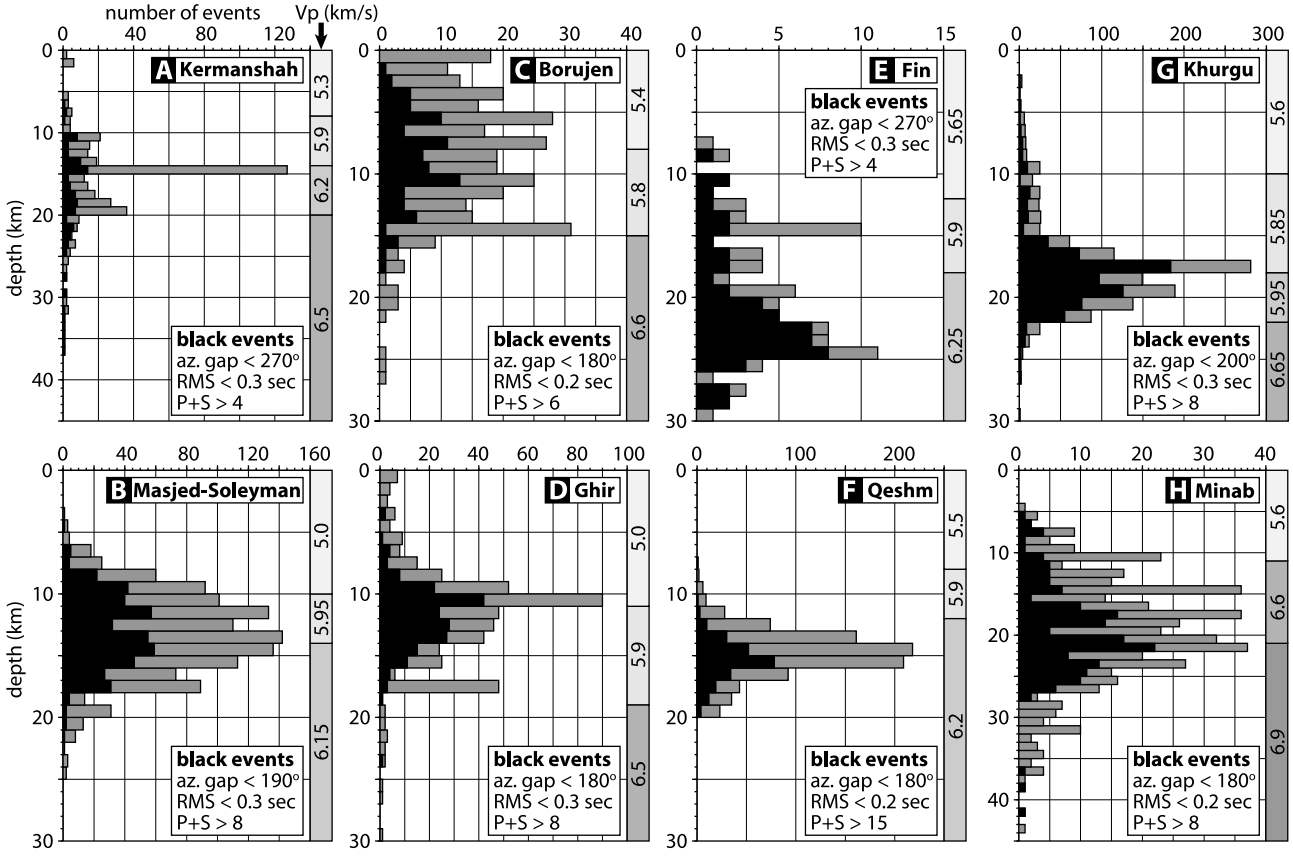

Figure 5. Histograms showing the depth distribution of locally recorded microseismicity in the eight regions plotted on Fig. 1(b) (note the different vertical scale in A and H). Black bars represent the best-recorded events with the most reliable depths, selected according to the azimuthal gap (*az. gap*), RMS residual (RMS) and the number of separate *P* and *S* phase recordings (*P*+*S*). Grey bars represent those that were less well-recorded. The minimum-misfit local 1-D velocity structure is shown on the right-hand side of each plot.

4 TELESEISMICALLY RECORDED EARTHQUAKES

In this section, we examine an updated catalogue of 202 earthquakes whose source parameters have been determined from teleseismic waveforms. These earthquakes are plotted on Figs 3 and 4, and their source parameters, together with the sources of the data, are listed in full in the supplementary material (Table S1). The earthquakes span the period 1957–2010, and their magnitudes mostly lie in the range M_w5.0–6.7, although there are a few smaller events of M_w 4.7–4.9. Only two earthquakes from 1957–1959 and eight from 1960–1969 are included, and the data set is not complete for these early years, particularly for smaller events of $M_w < 5.5$. We begin by outlining the accuracy of epicentres and the quality of focal mechanisms and centroid depths. We then discuss patterns shown in the earthquake data, building on earlier work by Talebian & Jackson (2004) but also making a series of significant new observations.

4.1 Sources of data

4.1.1 Epicentres

For eight earthquakes in the Fars Arc (Lohman & Simons 2005; Peyret *et al.* 2008; Roustaei *et al.* 2010; Nissen *et al.* 2010), InSAR observations provide very accurate coseismic fault locations. Eleven smaller (M_w 4.7–5.4) aftershocks are plotted at epicentres determined relative to the 2005 November 27 Qeshm and 2006 March 25 Fin mainshocks using hypocentroidal decomposition methods (Jordan & Sverdrup 1981). These epicentres are likely to be accurate to within ∼5 km, relative to the mainshock faulting (Roustaei *et al.* 2010; Nissen *et al.* 2010). The remaining earthquakes are plotted at their EHB epicentres [Engdahl *et al.* (1998) and its subsequent updates], with the exception of seven of the most recent earthquakes (spanning 2008–2010) which do not yet have EHB epicentres and are instead plotted at their USGS PDE locations. From a comparison with the eight fault locations determined using InSAR, errors in EHB and USGS PDE epicentres are up to ∼20 km, and on average ∼10 km.

4.1.2 Source parameters

For 65 of the earthquakes, plotted in black in Figs 3 and 4, source mechanisms and centroid depths are available from full *P* and *SH* waveform modelling. These include 12 new focal mechanisms outlined in Table 1, in addition to those published by Baker (1993), Baker *et al.* (1993), Priestley *et al.* (1994), Maggi *et al.* (2000), Walker (2003), Talebian & Jackson (2004), Walker *et al.* (2005), Peyret *et al.* (2008), Roustaei *et al.* (2010) and Nissen *et al.* (2010). For most of these studies (including this one), source parameters were determined by minimizing the misfit between observed *P* and *SH* waveforms recorded by long-period GDSN stations in the range 30°–90°, and synthetic waveforms computed for a point source embedded in an elastic half-space (McCaffrey & Abers 1988; Zwick *et al.* 1994). This methodology is now routine for studies of this

Table 1. New earthquake source parameters from modelling *P* and *SH* body-waves (full models are shown in the Supplementary Material). *Latitude* and *Longitude* are from an updated version of Engdahl *et al.* (1998), except for the most recent two events for which USGS PDE epicentres are listed, and *Z* is the centroid depth in kilometres.

Date	Time	Latitude	Longitude	Strike 1	Dip 1	Rake 1	Strike 2	Dip 2	Rake 2	Z (km)	Moment (N m)	Mw	Fig.
2001 March 23	05:24	32.984°	46.636°	337	10	126	121	82	84	7	7.4×10^{16}	5.2	S9
2001 April 03	17:36	32.551°	48.022°	281	52	85	110	38	97	9	2.4×10^{16}	4.9	S10
2002 April 24	19:48	34.602°	47.401°	294	71	139	39	52	24	3	9.1×10^{16}	5.2	S11
2002 September 25	22:28	32.064°	49.318°	310	44	82	142	47	98	8	1.2×10^{17}	5.3	S12
2002 December 24	17:03	34.542°	47.476°	311	27	98	122	63	86	5	2.6×10^{16}	4.9	S13
2003 February 14	10:29	28.006°	56.790°	312	25	115	105	67	79	23	9.1×10^{16}	5.2	S14
2003 July 10	17:40	28.248°	54.080°	313	67	88	138	23	95	5	2.6×10^{17}	5.5	S15
2006 February 28	07:31	28.133°	56.821°	302	12	113	99	79	85	15	1.0×10^{18}	5.9	S16
2008 August 27	21:52	32.31°	47.35°	338	88	192	248	78	358	10	3.0×10^{17}	5.6	S17
2010 July 20	19:38	26.77°	54.00°	317	26	87	140	64	91	5	4.3×10^{17}	5.7	S18
2010 September 27	11:22	26.67°	51.66°	280	13	71	119	78	94	16	4.3×10^{17}	5.6	S19
2010 November 26	12:33	28.11°	52.53°	295	41	86	120	49	93	4	1.4×10^{17}	5.4	S20

type, and is described in detail elsewhere (e.g. Molnar & Lyon-Caen 1989; Talebian & Jackson 2004).

The remaining earthquakes, plotted in grey, include 23 focal mechanisms constrained from long-period *P*-wave first motions (Shirakova 1967; McKenzie 1972; Kadinsky-Cade & Barazangi 1982; Jackson & McKenzie 1984; Ni & Barazangi 1986), and 114 Global CMT catalogue mechanisms determined from low-pass filtered, long-period body-waves and surface waves. First motions mechanisms are considered less reliable, particularly for thrust or reverse-faulting events, for which the *SH* nodal planes provide important constraints. Of these earthquakes, 33 have independently determined centroid depths plotted next to the focal sphere. These depths were determined from *P* and/or *SH* depth phases (Jackson & Fitch 1981; Kadinsky-Cade & Barazangi 1982; Ni & Barazangi 1986; Maggi *et al.* 2000; Adams *et al.* 2009) or by modelling small surface-deformation signals observed with InSAR (Lohman & Simons 2005).

For the mechanisms determined by *P* and *SH* body-wave modelling, realistic uncertainties can be estimated by visually assessing how far each source parameter can be shifted from its minimum-misfit value before the fit between observed and synthetic waveforms deteriorates (Molnar & Lyon-Caen 1989). For larger earthquakes, errors are generally $\sim 10^\circ$ for strike and dip and $\sim 20^\circ$ in rake, while for smaller earthquakes ($M_w < 5.5$) the uncertainties are somewhat larger owing to the sparser station coverage.

Errors in centroid depth calculated this way are typically ± 2 km, although an additional uncertainty arises if the assumed half-space velocities are inaccurate. In particular, most previous workers [Talebian & Jackson (2004) and references within] assumed an average V_p of 6.0–6.5 km s^{-1} above the source, whereas the most recent papers (including this one) make use of the velocities calculated by inverting locally recorded earthquake arrival times, which are generally 5.0–5.6 km s^{-1} in the uppermost 10–15 km. A slower half-space velocity requires a shallower centroid depth to maintain the temporal separation between direct arrivals (*P* and *S*) and surface reflections (*pP*, *sP*, *sS*). For the 10 earthquakes modelled here, we found that reducing V_p from 6.5 km s^{-1} to values consistent with the microseismic surveys (5.0–5.6 km s^{-1}) makes the centroid depth shallower by 1–2 km. This implies that depths reported by Talebian & Jackson (2004) may be systematically too deep by up to 1–2 km.

4.2 Strike-slip faulting

We do not have much to add to the observations made by Talebian & Jackson (2004) on the role of strike-slip faulting within the Zagros, as there have been only a few additional strike-slip earthquakes since 2000. The largest of the new events was the 2006 March 31 Chalan-Chulan earthquake (M_w 6.0, Fig. 1), discussed in detail by Peyret *et al.* (2008). This ruptured the section of the MRF between the 1958 August 16 Firuzabad earthquake (M_w 6.6) and the 1909 January 23 Silakhor earthquake (M_s 7.4). We provide source parameters of a M_w 5.2 strike-slip earthquake (2002 April 24) that occurred NW of the Firuzabad earthquake, which probably also involved right-lateral slip along the MRF (Fig. 4 and Table 1). The centroid depth of 3 km (with an estimated error of ± 2 km) suggests that slip in this earthquake may have reached the surface, but we do not know of any reports of surface rupturing.

The largest strike-slip event modelled in this study is a M_w 5.6 earthquake (2008 August 27) in the south-western Dezful Embayment, close to the ZFF (Fig. 4 and Table 1). Due to the lack of NE-trending structures in this region, we suspect it involved right-lateral slip on a vertical, NW-trending fault plane. The centroid depth of 10 km is consistent with rupture in the basement or the lower part of the sedimentary cover, and slip is unlikely to have broken the surface. This was the second earthquake of this orientation along the NW Zagros deformation front, an earlier M_w 5.3 event (2002 June 18) having occurred $\sim$150 km to the NW (we were unable to obtain improved source parameters for this earthquake, and the CMT solution is shown in Fig. 4). Recent GPS results indicate that the slip rate on the MRF may not be sufficient to account for all of the right-lateral component of Arabia–Iran motion (Walpersdorf *et al.* 2006), and these earthquakes suggest that a proportion of the remainder might be taken up along the deformation front.

4.3 Thrust faulting

As was noted in earlier papers (e.g. Talebian & Jackson 2004), there are only a small number of thrust earthquakes in the High Zagros (Figs 3 and 4). The few that are recorded here are situated along the south-eastern section of the HZF (Fig. 3c), although locally recorded events also support activity of this fault near Kermanshah, as discussed in Section 3. Instead, most thrust earthquakes occur within the SFB, where their orientation mimics that of the range

itself, striking NW–SE from the Lurestan Arc through to the western Fars Arc and E–W in the central and eastern Fars Arc. As pointed out by Talebian & Jackson (2004), they are mostly restricted to areas of low topography (with smoothed elevations of less than 1250 m), up to ∼150 km from the foreland. However, there is no concentration of events along the deformation front itself, and out-of-sequence thrusting is common. It is especially notable that seismicity appears absent from ∼400 km section of the ZFF near Ahvaz, with earthquakes instead clustered along the northern margin of the Dezful Embayment (Fig. 4). Some of the earthquakes lie close to the major basement thrusts documented by Berberian (1995), forming apparent lineaments along the Surmeh fault (Fig. 3), the easternmost MFF (Fig. 3c) and the frontal Lurestan Arc (Fig. 4).

Nodal planes typically dip at 30°–60°; even accepting the ambiguity in which nodal plane represents faulting, low-angle thrusting is relatively rare. Jackson (1980) suggested that these steep dips were inherited from older normal faults in the stretched Arabian margin. On a regional scale there is no evidence for a seismically active decollement as is observed beneath the Himalaya, although low-angle thrusting may play an important role in a couple of areas. First, scattered low-angle thrusts occur at more than one level in and around the Dezful Embayment (see centroid depths of 5 km, 14 km and 17 km in Fig. 4). The second area is the far SE Zagros, the only place in the entire range where teleseismically-recorded earthquakes occur at depths greater than ∼20 km—two at 28 km and a new M_w 5.2 event (2003 February 14) at 23 km (Fig. 3c and Table 1). These three mechanisms are consistent with slip on shallow, N-dipping planes, and probably represent local underthrusting of the Arabian basement beyond the surface expression of the geological suture (MZRF) beneath central Iran, where the Zagros is at its narrowest (Talebian & Jackson 2004).

Histograms of centroid depths are shown in Figs 6(a) and (b), where earthquakes are coloured according to mechanism (grey for thrust, black for strike-slip) and separated by area (the SFB on the left, and the High Zagros on the right). Except for the three low-angle thrusts in the far SE Zagros (discussed earlier), reverse faulting earthquakes have centroid depths of between 4 km and 20 km. Within the SFB, three quarters of the centroid depths are at 4–10 km (Fig. 6a). Considering that many earthquakes may actually be 1–2 km shallower—having been determined using unrealistically high seismic velocities (Section 4.1.2)—the majority of the earthquakes within the SFB probably lie within the sedimentary cover, contrary to the conclusions of earlier papers that place most within the basement (e.g. Jackson 1980; Maggi *et al.* 2000; Talebian & Jackson 2004; Hatzfeld *et al.* 2010). Only the relatively small number of earthquakes with centroid depths greater than 15 km can be attributed to basement faulting with certainty. These deepest events imply a seismogenic layer thickness of ∼20 km, consistent with many of the estimates from local seismicity though slightly smaller than the 25–30 km values at Kermanshah, Fin and Khurgu (Fig. 5).

5 DISCUSSION

5.1 The Qeshm and Fin earthquakes revisited

Key evidence for the nature of faulting within the sedimentary cover comes from recent InSAR studies of the 2005 November 27 and 2008 September 10 Qeshm earthquakes [M_w 5.8 and 5.9; Nissen *et al.* (2007, 2010)] and the 2006 March 25 Fin earthquakes [M_w 5.7 and 5.5; Roustaei *et al.* (2010)]. Both earthquakes occurred in areas of gentle, symmetric folds, of the sort normally ascribed to detachment folding. At both Qeshm and Fin, Neogene strata of the Bakhtyari, Agha Jari and Mishan formations are exposed at the surface (Fig. 2).

First, because the wavelength of the surface deformation is sensitive to the depth of rupture, elastic dislocation modelling yielded accurate top and bottom depths of the earthquake faulting. None of these earthquakes produced surface ruptures, with the up-dip limit of slip occurring at depths of ∼3–5 km, corresponding to the level of the Cretaceous Gurpi marl formation. The base of the ruptures coincided with the expected level of the Hormuz salt at depths of ∼8–10 km, hinting that this weak layer formed a barrier at the base of the sedimentary cover across which slip failed to propagate. These rupture depths also provide further confirmation that the lower sedimentary cover is capable of producing moderate-sized earthquakes (M_w 5–6) even away from the south-verging, asymmetric folds highlighted by Berberian (1995).

Secondly, the resulting maps of coseismic surface deformation were compared with the position and orientation of surface folding. The area uplifted during the Fin earthquakes trends ENE, oblique to the overlying E–W fold axes, while the Qeshm earthquakes ruptured a SSE-dipping fault, perpendicular to the trace of the overlying anticline. In neither case is there a clear connection between the causative faulting and the overlying folding, probably due to a detachment in the Gurpi marls. These results show that surface anticlines in these epicentral areas form by detachment folding, rather than by forced folding above discrete thrusts. Detachment folding is probably the dominant mode of surface fold generation in other regions of open, symmetric folding across the SFB, although additional geodetic studies of future earthquakes would help to confirm this. Nevertheless, forced folding does also occur in some specific areas, as we shall discuss in Section 5.2.

Perhaps the most surprising aspect of the earthquakes at Qeshm and Fin was the high concentration of well-resolved, locally recorded aftershocks within the basement, below the level of mainshock faulting. Possible triggering mechanisms include Coulomb stress changes and the effects of loading or shaking. To explore these possibilities, we computed Coulomb stress changes for the 2005 November 27 Qeshm mainshock using the USGS Coulomb 3.2 software (Lin & Stein 2004; Toda *et al.* 2005). This analysis is shown in full in the Supplementary Material, and the results are inconclusive: many of the basement aftershocks occurred in areas where faults were brought closer to failure (by up to ∼0.1 MPa, but more typically <0.05 MPa), but a small number also occurred in areas where Coulomb stresses would act to inhibit faulting. Loading effects can only account for even smaller stress changes in the basement, of less than ∼0.03 MPa (using the relationship $\Delta P = \rho g \Delta h$, where ΔP is the change in lithostatic pressure, ρ is the density, g is standard gravity and Δh is the slip, assumed from scaling relations to be less than 1 m). It therefore appears likely that other triggering mechanisms, such as dynamic stress transfer caused by shaking, must also play a role.

5.2 Earthquake magnitudes and seismic hazard

In many ways, the Qeshm and Fin earthquakes are typical of the seismicity of the SFB, involving slip on steep reverse faults and moment magnitudes of 5.5–6.0. In fact, it is conspicuous that there are very few thrust-faulting earthquakes in the SFB with significantly larger magnitudes, the majority being of $M_w \leq 6.1$ (Fig. 6c).

Empirical scaling relations show that intraplate earthquake slip-to-length ratios (u/L) are typically $\sim 5 \times 10^{-5}$ (Scholz 1982), and

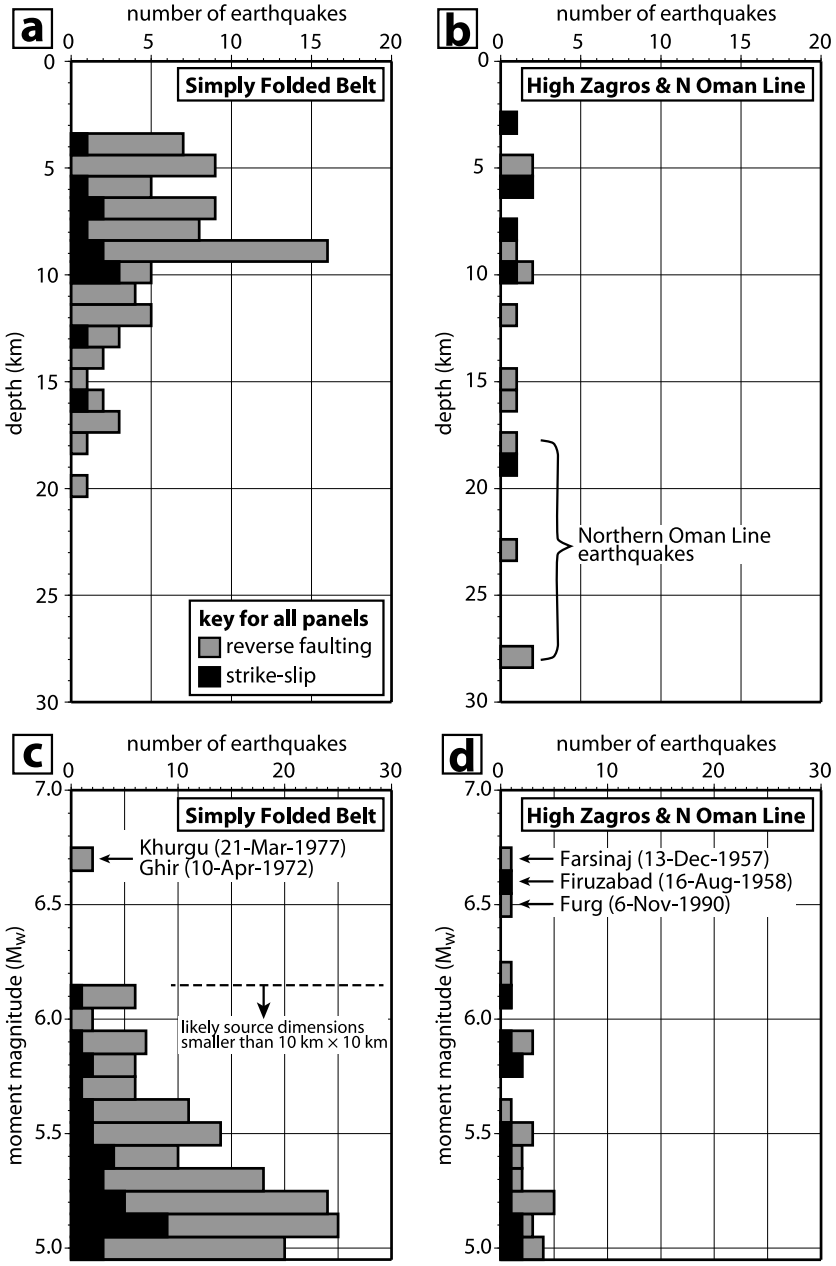

Figure 6. Histograms showing the centroid depths (upper panels) and magnitudes (lower panels) of teleseismically recorded earthquakes in the Simply Folded Belt (left-hand side) and the High Zagros and northern Oman Line (right-hand side). Strike-slip events are marked in black, and dip-slip events in grey. The Simply Folded Belt earthquakes comprise all those that lie south of the HZF; the High Zagros earthquakes include those lying between the HZF and the MZRF/MRF, as well as the cluster of events north of the easternmost MZRF along the northern Oman Line (see NE part of Fig. 3c).

from the relationship $M_o = \mu Au$ (where A is the area and μ the elastic rigidity) the expected source dimensions of an earthquake can be calculated. An earthquake of M_w 6.1 corresponds to a length and width of about 10 km. Using a dip of 30°–60°, a thrust earthquake of this magnitude would rupture a layer 5–9 km thick. These source dimensions can be contained within the Competent Group (as demonstrated by the Qeshm and Fin earthquakes), or within the seismogenic part of the basement. The prevalence of moderately sized earthquakes in the SFB hints that there are important regional barriers to vertical rupture propagation, certainly at the base of the cover (the Hormuz salt) and possibly in the middle and upper parts of the cover as well (e.g. Gurpi marls, Gachsaran evaporites).

The typical maximum earthquake magnitude of about 6.1 is also observed in areas where there is no known Hormuz salt (Fig. 6c), lending weight to suggestions that this salt layer either continues into the Dezful Embayment and Lurestan Arc or is replaced by another weak horizon (McQuarrie 2004; Sherkati & Letouzey 2004; Carruba *et al.* 2006). We do note, though, that there might be other plausible limiting factors to earthquake magnitude. For instance, if thrusts in the SFB reactivate normal faults derived from earlier periods of rifting (Jackson 1980) then the segmentation length of these inherited structures might limit the maximum fault area available to rupture.

With the same assumptions, a thrust earthquake of $M_w > 6.7$ would have likely source dimensions of about 20 × 20 km, and is

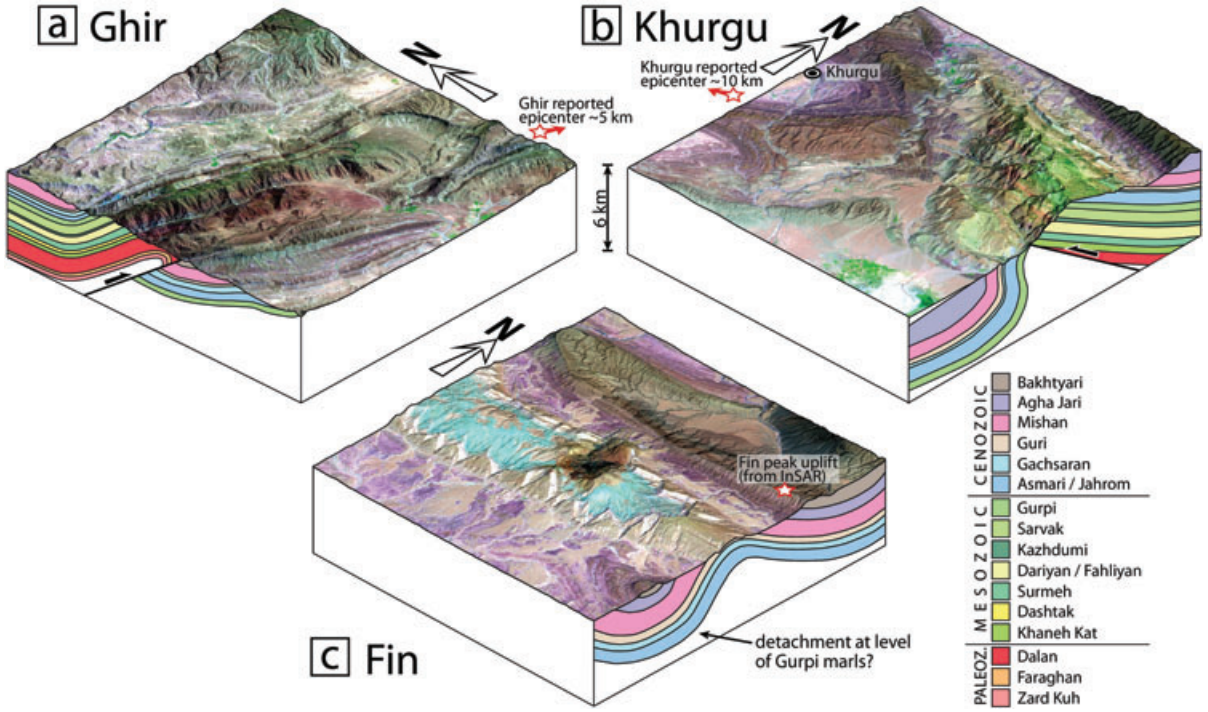

Figure 7. Perspective views (Landsat RGB 742 draped on G-DEM topography) of folding in the (a) Ghir, (b) Khurgu and (c) Fin regions, with structural interpretations based on geological maps, digital topography and a cross-section of the Kuh-e-Kush anticline by (Sherkati *et al.* 2005). There is no vertical exaggeration. The locations of these maps are plotted on Fig. 3.

therefore difficult to contain within the Competent Group. There are only two instrumentally recorded thrust faulting earthquakes in the SFB of this magnitude—those at Ghir (1972 April 10) and Khurgu (1977 March 21). There are very few events with such large magnitudes in the historical record of the SFB, and no clear historical evidence for any earthquake greater than M ∼7 (Ambraseys & Melville 1982).

The 1972 Ghir earthquake produced maximum macroseismic intensities along the ESE-trending, southward-verging Surmeh anticline (Dewey & Grantz 1973), which forms the southern termination of the right-lateral Kareh Bas fault, and contains in its core the only exposures of Ordovician strata in the whole SFB (Fig. 7a). The earthquake had a moment magnitude (M_w) of ∼6.7 and a centroid depth of ∼9 km, estimated from *P* and *SH* body-waveform modelling (Baker *et al.* 1993). The location of the 1977 Khurgu earthquake is less well constrained, but the greatest reported shaking (at the village of Khurgu) occurred close to the Kush Kuh anticline (Nowroozi *et al.* 1977), a SW-verging fold positioned at the SE end of the High Zagros Fault which exposes Lower Mesozoic strata in its core (Fig. 7b). The earthquake has a published Global CMT moment magnitude of 6.7 and a centroid depth of ∼12 km, established using *P*-wave depth phases (Jackson & Fitch 1981). Diffuse aftershock microseismicity detected by an array of portable seismometers was concentrated between depths of 4–22 km (Nowroozi *et al.* 1977).

Given their centroid depths and likely source dimensions, the M_w 6.7 Ghir and Khurgu earthquakes probably affected both basement and sediments, rupturing through the basement–cover interface. Both also occurred in special locations, near strongly asymmetric anticlines which expose otherwise rare Palaeozoic or Lower Mesozoic strata at the surface and which accommodate large steps in stratigraphic level (Figs 7a and b). These anticlines are geomorphologically distinct from the open, symmetric folds which characterize most of the SFB, such as the epicentral region of the Fin earthquakes (Fig. 7c), where incompetent layers limit earthquakes to moderate magnitudes ($M_w \sim 6$) and detach the surface folding from reverse faults in the lower part of the cover.

Folds of the kind associated with the Ghir and Khurgu earthquakes represent the most significant seismic hazard in the SFB, as they are probably the only places where such large events can be generated. Anticlines displaying similar asymmetries and deep exposures are relatively rare, but there are a few other examples including parts of the frontal MFF (such as 27.5°N, 52.5°E) and the Kuh-e-Muran anticline (27.7°N, 55.5°E) in the north-eastern Fars Arc (Leturmy *et al.* 2010). These folds are each several 10s of kilometres in length, but cannot be traced along the full length of the range in the sense depicted in the 'master blind thrust' model of Berberian (1995).

5.3 Seismic versus aseismic deformation

One aspect of the Zagros which remains poorly understood is the mismatch between the rate of strain released seismically and the overall motions accommodated across the range. This discrepancy was first recognized by Jackson & McKenzie (1988), who found that the summed moment tensors of 17 $M \geq 6.0$ earthquakes spanning the interval 1909–1978 could account for just 4–7 per cent of the expected shortening across the range, assuming a seismogenic layer thickness of 15 km. However, their calculation utilized Arabia–Iran convergence rates (∼10–30 mm yr^{-1}) which exceed those determined from GPS measurements by a factor of ∼3. Masson *et al.* (2005) repeated the calculation using strain rates obtained from GPS and an earthquake record updated to 2002. Assuming a seismogenic thickness of 15 km, they found a large regional variation in the seismic contribution, from a minimum of 2 per cent (in the Dezful Embayment) to a maximum of 22 per cent (in the SE Fars

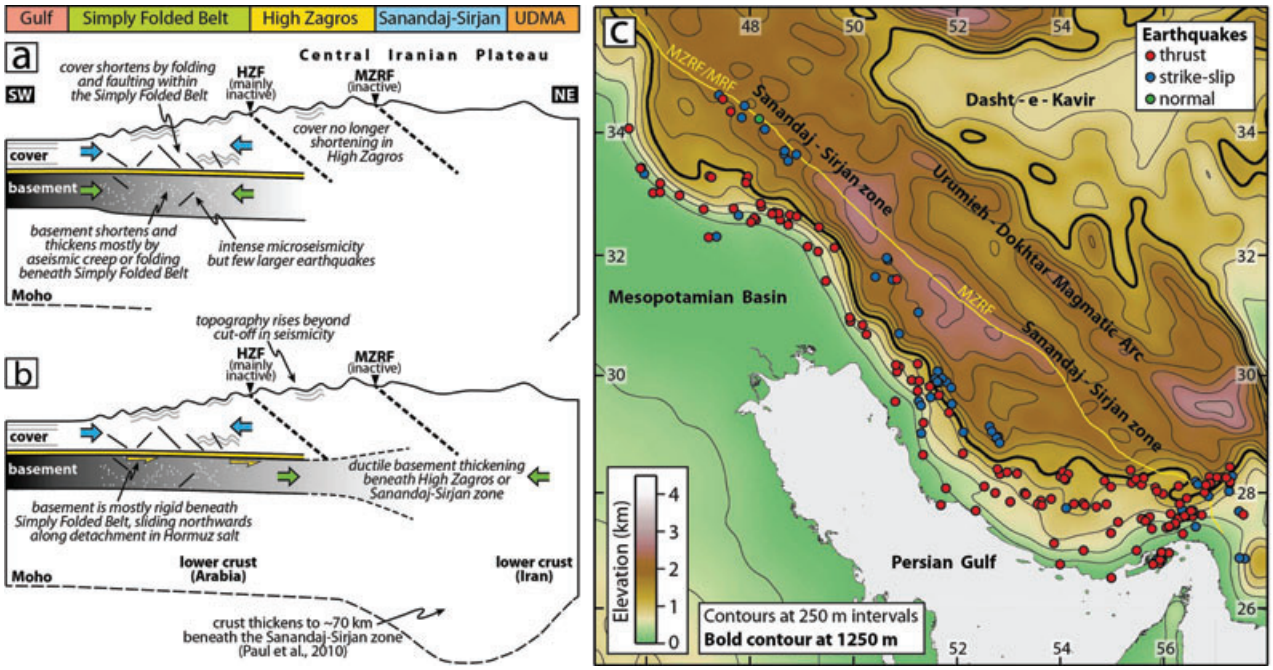

Figure 8. (a) and (b) Schematic cross-sections showing possible mechanisms for the shortening of the Zagros basement. In (a), the seismogenic basement mainly deforms by aseismic fault creep or folding (accompanied by high levels of microseismicity and rare larger earthquakes) beneath the Simply Folded Belt. In (b), the basement remains mostly rigid beneath the Simply Folded Belt, passing northwards along a low-angle detachment to deform in a ductile manner beneath the High Zagros or the Sanandaj-Sirjan zone. (c) Smoothed topography and teleseismically recorded earthquake epicentres in the Zagros. The topography was smoothed using a Gaussian filter with a radius of 50 km, and is contoured at 500 m intervals with the 1250 m contour highlighted in bold. Earthquakes are the same as those plotted in Figs 3 and 4 and are coloured according to mechanism.

Arc). Masson *et al.* (2005) also noted that the principal components of the horizontal seismic strain-rate field have similar orientations to those calculated from the GPS-determined strain field, so there is no need for the missing aseismic deformation to differ in position or orientation from that released in earthquakes.

From earthquake magnitude–frequency relations (e.g. Scholz & Cowie 1990), the contribution of moderate events of M_w 5.0–5.9 will roughly double the seismic strain rate estimated from earthquakes of $M_w \geq 6.0$, if the largest earthquakes are M_w 6.7. This is confirmed by the teleseismically recorded earthquakes listed in the supplementary material (Table S1), for which events of $M_w <$ 6.0 account for 44 per cent of the total moment released since the Global CMT catalogue was introduced in 1976. Taking these moderate-sized events into consideration, earthquakes can account for ~30 per cent of the overall strain rate for a seismogenic layer of thickness 15 km (or all of the shortening of a layer of thickness ~5 km). It is implausible that this mismatch results from an unrepresentative sample of long-term seismicity—the deficit amounts to a missing Ghir/Khurgu-type earthquake every 2–3 years, which would surely have been noted in the historical record (Ambraseys & Melville 1982).

Within the SFB, the distribution of teleseismic centroid depths shows that most seismic strain is released at depths of 5–10 km. If estimates of the thickness of the sedimentary cover of 10–14 km are correct (see Section 2.2), then most of these earthquakes occur within the lower sedimentary cover (Fig. 6a). Within the ~5 km-thick Competent Group, earthquakes can therefore account for most of the overall rate of shortening, though folding is obviously also important. In contrast, there are many fewer moderate-sized earthquakes (and much less seismic strain released) at depths of 10–20 km, and the basement of the Zagros must therefore be shortening mainly aseismically. For much of the Phanerozoic, the Zagros was a subsiding continental margin that was accumulating a thick package of sediments. Basins that become filled with sediments of low conductivity are able to retain high temperatures long after initial lithospheric stretching increases the geothermal gradient (McKenzie 1981; Jackson 1987), suggesting that the Arabian basement underlying the sediments of the Zagros may remain hot and weak. Nevertheless, it must be strong (or cold) enough to support pervasive microseismicity at depths of up to 20–30 km (Fig. 5), as well as rare larger earthquakes at depths of up to ~20 km (Fig. 6a). There are therefore a number of possible mechanisms that can account for these observations, although there are problems with each one:

(1) Aseismic fault creep or folding provides one viable mechanism for substatial shortening of the Arabian basement beneath the SFB (Fig. 8a). In California, high concentrations of microearthquakes are associated with faults that are known to be creeping (Rubin *et al.* 1999; Waldhauser & Ellsworth 2002). However, as discussed in Section 3, well-located basement microseismicity in the Zagros is rarely seen to be alligned along discrete fault structures, in the way observed in California.

(2) An alternative model allows the Arabian basement to remain mostly rigid beneath the SFB (thus accounting for the low seismic moment release at depths of 10–20 km), with aseismic shortening at this level instead occurring further north (Fig. 8b), either in the High Zagros or beneath the Sanandaj–Sirjan zone. Most moderate-to-large thrust earthquakes are restricted to low parts of the SFB, with average elevations of less than ~1250 m, but the topography continues to rise NE of this limit, only reaching its maximum elevation (2000–2500 m) along the MZRF (Fig. 8c). This further rise in topography may indicate aseismic shortening of the Arabian basement beneath the High Zagros; presumably the basement is deeper,

hotter and weaker here than it is beneath the SFB. It is possible that the Arabian basement remains rigid beneath the whole range, instead passing northwards and indenting weaker Iranian material beneath the Sanandaj–Sirjan zone (Fig. 8b), where the crust is known to be thickest (Rham 2009; Paul *et al.* 2010). These suggestions require a low-angle décollement with which to detach the sediments from the basement. Rare low-angle thrusting mechanisms provide some indication for such a structure, at least in places—such as the centroid depths of 14–17 km along the Balarud Line (Inset, Fig. 4) and centroid depths of 18–28 km along the Oman Line (Fig. 3c). However, the high-angle basement steps in places such as Ghir and Khurgu should disrupt any such detachment, making a single, ubiquitous décollement (of the kind depicted in critical wedge models) unlikely.

6 CONCLUSIONS

The integration of observations from a variety of sources—local network and teleseismic data, InSAR and geomorphology—reveals features of the deformation of the Zagros that were not apparent from previous studies that relied on single methods alone. The range is seismogenic to depths of ∼20 km, but most moderate-sized (M_w 5–6) earthquakes occur in the lower sedimentary cover (at depths of 5–10 km), not in the basement as had previously been thought. These faults have little or no surface expression as they are detached from surface folding by incompetent layers in the mid-cover. Weak Hormuz salt at the base of the cover is also important, breaking up faulting and limiting most earthquakes to $M_w \leq 6.0$. Only a few faults affect both basement and cover, and these are capable of generating larger earthquakes, up to at least M_w 6.7. These larger faults occur in particular places, beneath strongly asymmetric anticlines containing rare surface exposures of lower Mesozoic or Palaeozoic strata. While earthquakes can account for most of the shortening of the lower sedimentary cover, deformation at the level of the basement is largely aseismic. However, it is not clear whether the basement (1) shortens by fault creep and/or folding beneath the SFB, or (2) deforms in a ductile manner further north, beneath the High Zagros or the Sanandaj–Sirjan zone.

ACKNOWLEDGMENTS

The Center for the Observation and Modelling of Volcanoes, Earthquakes and Tectonics (COMET) is part of the National Center for Earth Observation (NCEO), and is supported by the Natural Environmental Research Council (NERC). We would like to thank E. R. Engdahl for giving us access to his updated EHB catalogue, Alex Copley, Tim Craig and Alastair Sloan for many useful discussions, and George Hilley and an anonymous reviewer for their helpful comments on the manuscript.

REFERENCES

Adams, A., Brazier, R., Nyblade, A., Rodgers, A. & Al Amri, A., 2009. Source parameters for moderate earthquakes in the Zagros mountains with implications for the depth extent of seismicity, *Bull. seism. Soc. Am.*, **99,** 2044–2049.

Al Amri, A.M. & Gharib, A.A., 2000. Lithospheric seismic structure of the eastern region of the Arabian Peninsula, *J. Geodyn.*, **29,** 125–139.

Al Damegh, K., Sandvol, E. & Barazangi, M., 2005. Crustal structure of the Arabian plate: new constraints from the analysis of teleseismic receiver functions, *Earth planet. Sci. Lett.*, **231,** 177–196.

Alavi, M., 2004. Regional stratigraphy of the Zagros fold-thrust belt of Iran and its proforeland evolution, *Am. J. Sci.*, **304,** 1–20.

Alavi, M., 2007. Structures of the Zagros fold-thrust belt in Iran, *Am. J. Sci.*, **307,** 1064–1095.

Allen, M.B. & Armstrong, H.A., 2008. Arabia Eurasia collision and the forcing of mid-Cenozoic global cooling, *Palaeogeog. Palaeoclim. Palaeoecol.*, **265,** 52–58.

Ambraseys, N.N. & Melville, C.P., 1982. *A History of Persian Earthquakes*, Cambridge University Press, Cambridge.

Aubourg, C., Smith, B., Bakhtari, H.R., Guya, N. & Eshraghi, A., 2008. Tertiary block rotations in the Fars Arc (Zagros, Iran), *Geophys. J. Int.*, **173,** 659–673.

Authemayou, C., Chardon, D., Bellier, O., Malekzadeh, Z., Shabanian, E. & Abbassi, M.R., 2006. Late Cenozoic partitioning of oblique plate convergence in the Zagros fold-and-thrust belt (Iran), *Tectonics*, **25,** TC3002, doi:10.1029/2005TC001860.

Authemayou, C. *et al.*, 2009. Quaternary slip-rates of the Kazerun and the Main Recent Faults: active strike-slip partitioning in the Zagros fold-and-thrust belt, *Geophys. J. Int.*, **178,** 524–540.

Bahroudi, A. & Koyi, H.A., 2003. Effect of spatial distribution of Hormuz salt on deformation style in the Zagros fold and thrust belt: an analogue modelling approach, *J. geol. Soc. Lond.*, **160,** 719–733.

Baker, C., 1993. The active seismicity and tectonics of Iran, *PhD thesis*, University of Cambridge.

Baker, C., Jackson, J. & Priestley, K., 1993. Earthquakes on the Kazerun Line in the Zagros Mountains of Iran: strike-slip faulting within a fold-and-thrust belt, *Geophys. J. Int.*, **115,** 41–61.

Berberian, M., 1995. Master blind thrust faults hidden under the Zagros folds: active basement tectonics and surface morphotectonics, *Tectonophysics*, **241,** 193–224.

Blanc, E.J.-P., Allen, M.B., Inger, S. & Hassani, H., 2003. Structural styles in the Zagros Simple Folded Zone, Iran, *J. geol. Soc. Lond.*, **160,** 401–412.

Carruba, S., Perotti, C.R., Buonaguro, R., Calabrò, R., Carpi, R. & Naini, M., 2006. Structural pattern of the Zagros fold-and-thrust belt in the Dezful Embayment (SW Iran), *Geol. Soc. Am. Spec. Pap.*, **414,** 11–32.

Casciello, E., Vergés, J., Saura, E., Casini, G., Fernández, N., Blanc, E., Homke, S. & Hunt, D.W., 2009. Fold patterns and multilayer rheology of the Lurestan Province, Zagros Simply Folded Belt (Iran), *J. geol. Soc. Lond.*, **166,** 947–959.

Colman-Sadd, S.P., 1978. Fold development in Zagros simply folded belt, Southwest Iran, *Am. Assoc. Petrol. Geol. Bull.*, **62,** 984–1003.

Dewey, J.W. & Grantz, A., 1973. The Ghir earthquake of April 10, 1972 in the Zagros mountains of southern Iran: seismotectonic aspects and some results of a field reconnaissance, *Bull. seism. Soc. Am.*, **63,** 2071–2090.

Emami, H., Vergés, J., Nalpas, T., Gillespie, P., Sharp, I., Karpuz, R., Blanc, E.P. & Goodarzi, M.G.H., 2010. Structure of the Mountain Front Flexure along the Anaran anticline in the Pusht-e-Kuh Arc (NW Zagros, Iran): insights from sand box models, *Geol. Soc. Lond. Spec. Publ.*, **330,** 155–178.

Engdahl, E.R., van der Hilst, R.D. & Buland, R., 1998. Global teleseismic earthquake relocation from improved travel times and procedures for depth determination, *Bull. seism. Soc. Am.*, **88,** 722–743.

Fakhari, M.D., Axen, G.J., Horton, B.K., Hassanzadeh, J. & Amini, A., 2008. Revised age of proximal deposits in the Zagros foreland basin and implications for Cenozoic evolution of the High Zagros, *Tectonophysics*, **451,** 170–185.

Falcon, N.L., 1969. Problems of the relationship between surface structure and deep displacements illustrated by the Zagros Range, *Geol. Soc. Lond. Spec. Publ.*, **3,** 9–21.

Falcon, N.L., 1974. Southern Iran: Zagros Mountains, *Geol. Soc. Lond. Spec. Publ.*, **4,** 199–211.

Gavillot, Y., Axen, G.J., Stockli, D.F., Horton, B.K. & Fakhari, M.D., 2010. Timing of thrust activity in the High Zagros fold-and-thrust belt, Iran, from (U-Th)/He thermochronometry, *Tectonics*, **29,** TC4025, doi:10.1029/2009TC002484.

Gholamzadeh, A., Yamini-Fard, F., Hessami, K. & Tatar, M., 2009. The February 28, 2006 Tiab earthquake, Mw 6.0: implications for tectonics of the transition between the Zagros continental collision and the Makran subduction zone, *J. Geodyn.*, **47,** 280–287.

Gök, R., Mahdi, H., Al Shukri, H. & Rodgers, A.J., 2008. Crustal structure of Iraq from receiver functions and surface wave dispersion: implications for understanding the deformation history of the Arabian-Eurasian collision, *Geophys. J. Int.*, **172,** 1179–1187.

Hatzfeld, D., Tatar, M., Priestley, K. & Ghafory-Ashtiany, M., 2003. Seismological constraints on the crustal structure beneath the Zagros Mountain belt (Iran), *Geophys. J. Int.*, **155,** 403–410.

Hatzfeld, D. *et al.*, 2010. The kinematics of the Zagros Mountains (Iran), *Geol. Soc. Lond. Spec. Publ.*, **330,** 19–42.

Hessami, K., Koyi, H.A. & Talbot, C.J., 2001a. The significance of strike-slip faulting in the basement of the Zagros fold and thrust belt, *J. Petr. Geol.*, **24,** 5–28.

Hessami, K., Koyi, H.A., Talbot, C.J., Tabasi, H. & Shabanian, E., 2001b. Progressive unconformities within an evolving foreland fold thrust belt, Zagros Mountains, *J. geol. Soc. Lond.*, **158,** 969–981.

Homke, S., Vergés, J., Garcés, M., Emami, H. & Karpuz, R., 2004. Magnetostratigraphy of Miocene Pliocene Zagros foreland deposits in the front of the Push-e Kush Arc (Lurestan Province, Iran), *Earth planet. Sci. Lett.*, **225,** 397–410.

Husseini, M.I., 1992. Upper Palaeozoic tectono-sedimentary evolution of the Arabian and adjoining plates, *J. geol. Soc. Lond.*, **149,** 419–429.

Jackson, J. & Fitch, T., 1981. Basement faulting and the focal depths of the larger earthquakes in the Zagros mountains (Iran), *Geophys. J. Int.*, **64,** 561–586.

Jackson, J. & McKenzie, D., 1984. Active tectonics of the Alpine-Himalayan Belt between western Turkey and Pakistan, *Geophys. J. Int.*, **77,** 185–264.

Jackson, J. & McKenzie, D., 1988. The relationship between plate motions and seismic moment tensors, and the rates of active deformation in the Mediterranean and Middle East, *Geophys. J. Int.*, **93,** 45–73.

Jackson, J.A., 1980. Reactivation of basement faults and crustal shortening in orogenic belts, *Nature*, **283,** 343–346.

Jackson, J.A., 1987. Active continental deformation and regional metamorphism, *Phil. Trans. R. Soc. Lond. A*, **321,** 47–63.

Jahani, S., Callot, J.-P., Frizon de Lamotte, D., Letouzey, J. & Leturmy, P., 2007. The salt diapirs of the Eastern Fars Province (Zagros, Iran): a brief outline of their past and present, in *Thrust Belts and Foreland Basins*, pp. 289–308, Springer, Berlin.

Jahani, S., Callot, J.-P., Letouzey, J. & Frizon de Lamotte, D., 2009. The eastern termination of the Zagros Fold-and-Thrust Belt, Iran: structures, evolution, and relationships between salt plugs, folding, and faulting, *Tectonics*, **28,** TC6004, doi:10.1029/2008TC002418.

James, G.A. & Wynd, J.G., 1965. Stratigraphic Nomenclature of Iranian Oil Consortium Agreement Area, *Am. Assoc. Petrol. Geol. Bull.*, **49,** 2182–2245.

Jordan, T.H. & Sverdrup, K.A., 1981. Teleseismic location techniques and their application to earthquake clusters in the South-Central Pacific, *Bull. seism. Soc. Am.*, **71,** 1105–1130.

Kadinsky-Cade, K. & Barazangi, M., 1982. Seismotectonics of Southern Iran: the Oman Line, *Tectonics*, **1,** 389–412.

Kent, P.E., 1979. The emergent Hormuz salt plugs of southern Iran, *J. Petr. Geol.*, **2,** 117–144.

Khadivi, S. *et al.*, 2010. Magnetochronology of synorogenic Miocene foreland sediments in the Fars arc of the Zagros Folded Belt (SW Iran), *Basin. Res.*, **22,** 918–932.

Kissling, E., 1988. Geotomography with local earthquake data, *Rev. Geophys.*, **26,** 659–698.

Koop, W.J. & Stoneley, R., 1982. Subsidence History of the Middle East Zagros Basin, Permian to Recent, *Phil. Trans. R. Soc. Lond. A*, **305,** 149–167.

Kugler, A., 1973. An interpretation of the Southwest Iran aeromagnetic survey, Unpublished 1205, Oil Service Company of Iran.

Leturmy, P., Molinaro, M. & Frizon de Lamotte, D., 2010. Structure, timing and morphological signature of hidden reverse basement faults in the Fars Arc of the Zagros (Iran), *Geol. Soc. Lond. Spec. Publ.*, **330,** 121–138.

Lin, J. & Stein, R.S., 2004. Stress triggering in thrust and subduction earthquakes and stress interaction between the southern San Andreas and nearby thrust and strike-slip faults, *J. geophys. Res.*, **109,** B02303, doi:10.1029/2003JB002607.

Lohman, R.B. & Simons, M., 2005. Locations of selected small earthquakes in the Zagros mountains, *Geochem. Geophys. Geosyst.*, **6,** Q03001, doi:10.1029/2004GC000849.

Maggi, A., Jackson, J.A., Priestley, K. & Baker, C., 2000. A re-assessment of focal depth distributions in southern Iran, the Tien Shan and northern India: do earthquakes really occur in the continental mantle?, *Geophys. J. Int.*, **143,** 629–661.

Masson, F., Chéry, J., Hatzfeld, D., Martinod, J., Vernant, P., Tavakoli, F. & Ghafory-Ashtian i, M., 2005. Seismic versus aseismic deformation in Iran inferred from earthquakes and geodetic data, *Geophys. J. Int.*, **160,** 217–226.

McCaffrey, R. & Abers, G., 1988. *SYN3: A Program for Inversion of Teleseismic Body Wave Forms on Microcomputers*, Air Force Geophysical Laboratory Technical Report, Hanscomb Air Force Base, MA.

McKenzie, D., 1972. Active tectonics of the mediterranean region, *Geophys. J. Int.*, **30,** 109–185.

McKenzie, D., 1981. The variation of temperature with time and hydrocarbon maturation in sedimentary basins formed by extension, *Earth planet. Sci. Lett.*, **55,** 87–98.

McQuarrie, N., 2004. Crustal scale geometry of the Zagros fold-thrust belt, Iran, *J. Struct. Geol.*, **26,** 519–535.

McQuarrie, N., Stock, J.M., Verdel, C. & Wernicke, B.P., 2003. Cenozoic evolution of Neotethys and implications for the causes of plate motions, *Geophys. Res. Lett.*, **30**(20), 2036, doi:10.1029/2003GL017992.

Molinaro, M., Leturmy, P., Guezou, J.-C., Frizon de Lamotte, D. & Eshraghi, S.A., 2005. The structure and kinematics of the southeastern Zagros fold-thrust belt, Iran: from thin-skinned to thick-skinned tectonics, *Tectonics*, **24,** TC3007, doi:10.1029/2004TC001633.

Molnar, P. & Lyon-Caen, H., 1989. Fault plane solutions of earthquakes and active tectonics of the Tibetan Plateau and its margins, *Geophys. J. Int.*, **99,** 123–154.

Morris, P., 1977. Basement structure as suggested by aeromagnetic surveys in SW Iran, Internal report, Oil Serivce Company of Iran.

Mouthereau, F., Tensi, J., Bellahsen, N., Lacombe, O., De Boisgrollier, T. & Kargar, S., 2007. Tertiary sequence of deformation in a thin-skinned/thick-skinned collision belt: the Zagros Folded Belt (Fars, Iran), *Tectonics*, **26,** TC5006, doi:10.1029/2007TC002098.

Murris, R.J., 1980. Middle East: stratigraphic evolution and oil habitat, *Am. Assoc. Petrol. Geol. Bull.*, **64,** 597–618.

Ni, J. & Barazangi, M., 1986. Seismotectonics of the Zagros continental collision zone and a comparison with the Himalayas, *J. geophys. Res.*, **91**(B8), 8205–8218.

Nissen, E., Ghorashi, M., Jackson, J., Parsons, P. & Talebian, M., 2007. The 2005 Qeshm Island earthquake (Iran) – a link between buried reverse faulting and surface folding in the Zagros Simply Folded Belt? *Geophys. J. Int.*, **171,** 326–338.

Nissen, E., Yamini-Fard, F., Tatar, M., Gholamzadeh, A., Bergman, E., Elliott, J.R., Jackson, J.A. & Parsons, B., 2010. The vertical separation of mainshock rupture and microseismicity at Qeshm island in the Zagros Simply Folded Belt, Iran, *Earth planet. Sci. Lett.*, **296,** 181–194.

Nowroozi, A.A., Ashjehi, A.M., Rad, M.R.S. & Izadpanah, A.A.Z., 1977. The mainshock and aftershocks of the Farvardin 2, 1356 earthquake in Khorgo region (in Farsi), technical report, Atomic Energy Authority of Iran.

O'Brien, C.A.E., 1957. Salt diapirism in south Persia, *Geologie en Mijnbouw*, **19,** 357–376.

Oberlander, T., 1965. *The Zagros Streams. A New Interpretation of Transverse Drainage in an Orogenic Zone*, Syracuse geograph. Ser. No. 1, 168pp, Syracuse University Press, Syracuse, NY.

Oveisi, B., Lavé, J., van der Beek, P., Carcaillet, J., Benedetti, L. & Aubourg, C., 2009. Thick- and thin-skinned deformation rates in the central Zagros simple folded zone (Iran) indicated by displacement of geomorphic surfaces, *Geophys. J. Int.*, **176,** 627–654.

Paul, A., Hatzfeld, D., Kaviani, A., Tatar, M. & Péquegnat, C., 2010. Seismic imaging of the lithospheric structure of the Zagros mountain belt (Iran), *Geol. Soc. Lond. Spec. Publ.*, **330,** 5–18.

Peyret, M., Rolandone, F., Dominguez, S., Djamour, Y. & Meyer, B., 2008. Source model for the Mw 6.1, 31 March 2006, Chalan-Chulan Earthquake (Iran) from InSAR, *Terra Nova*, **20,** 126–133.

Priestley, K., Baker, C. & Jackson, J., 1994. Implications of earthquake focal mechanism data for the active tectonics of the south Caspian Basin and surrounding regions, *Geophys. J. Int.*, **118,** 111–141.

Ramsey, L.A., Walker, R.T. & Jackson, J.A., 2008. Fold evolution and drainage development in the Zagros mountains of Fars province, SE Iran, *Basin. Res.*, **20,** 23–48.

Regard, V., Bellier, O., Thomas, J., Abbassi, M.R., Mercier, J., Shabanian, E., Feghhi, K. & Soleymani, S., 2004. Accommodation of Arabia-Eurasia convergence in the Zagros-Makran transfer zone, SE Iran: a transition between collision and subduction through a young deforming system, *Tectonics*, **23,** TC4007, doi:10.1029/2003TC001599.

Rham, D.J., 2009. The crustal structure of the middle East, *PhD thesis*, University of Cambridge.

Roustaei, M. *et al.*, 2010. The 25 March 2006 Fin earthquakes (Iran) – insights into the vertical extents of faulting in the Zagros Simply Folded Belt, *Geophys. J. Int.*, **181,** 1275–1291.

Rubin, A.M., Gillard, D. & Got, J., 1999. Streaks of microearthquakes along creeping faults, *Nature*, **400,** 635–641.

Scholz, C.H., 1982. Scaling laws for large earthquakes: consequences for physical models, *Bull. seism. Soc. Am.*, **72,** 1–14.

Scholz, C.H. & Cowie, P.A., 1990. Determination of total strain from faulting using slip measurements, *Nature*, **346,** 837–839.

Sepehr, M., Cosgrove, J. & Moieni, M., 2006. The impact of cover rock rheology on the style of folding in the Zagros fold-thrust belt, *Tectonophysics*, **427,** 265–281.

Sherkati, S. & Letouzey, J., 2004. Variation of structural style and basin evolution in the central Zagros (Izeh zone and Dezful Embayment), Iran, *Marine. Petr. Geol.*, **21,** 535–554.

Sherkati, S., Molinaro, M., Frizon de Lamotte, D. & Letouzey, J., 2005. Detachment folding in the Central and Eastern Zagros fold-belt (Iran): salt mobility, multiple detachments and late basement control, *J. Struct. Geol.*, **27,** 1680–1696.

Sherkati, S., Letouzey, J. & Frizon de Lamotte, D., 2006. Central Zagros fold-thrust belt (Iran): new insights from seismic data, field observation, and sandbox modeling, *Tectonics*, **25,** TC4007, doi:10.1029/2004TC001766.

Shirakova, E.I., 1967. General features in the orientation of principal stresses in earthquake foci in the Mediterranean-Asian seismic belt, *Earth Phys.*, **1,** 22–36.

Stöcklin, J., 1968. Structural history and tectonics of Iran: a review, *Am. Assoc. Petrol. Geol. Bull.*, **52,** 1229–1258.

Stöcklin, J., 1974. Possible ancient continental margins in Iran, in *The Geology of Continental Margins*, pp. 873–887, Springer-Verlag, New York, NY.

Stoneley, R., 1981. The geology of the Kuh-e-Dalneshin area of southern Iran and its bearing on the evolution of southern Tethys, *J. geol. Soc. Lond.*, **138,** 509–526.

Stoneley, R., 1990. The Arabian continental margin in Iran during the Late Cretaceous, *Geol. Soc. Lond. Spec. Publ.*, **49,** 787–795.

Talebian, M., 2003. Active faulting in the Zagros mountains of Iran, *PhD thesis*, University of Cambridge.

Talebian, M. & Jackson, J., 2002. Offset on the Main Recent Fault of NW Iran and implications for the late Cenozoic tectonics of the Arabia-Eurasia collision zone, *Geophys. J. Int.*, **150,** 422–439.

Talebian, M. & Jackson, J., 2004. A reappraisal of earthquake focal mechanisms and active shortening in the Zagros mountains of Iran, *Geophys. J. Int.*, **156,** 506–526.

Tatar, M., Hatzfeld, D. & Ghafory-Ashtiany, M., 2004. Tectonics of the Central Zagros (Iran) deduced from microearthquake seismicity, *Geophys. J. Int.*, **156,** 255–266.

Tavakoli, F. *et al.*, 2008. Distribution of the right-lateral strike slip motion from the Main Recent Fault to the Kazerun Fault System (Zagros, Iran): evidence from present-day GPS velocities, *Earth planet. Sci. Lett.*, **275,** 342–347.

Toda, S., Stein, R.S., Richards-Dinger, K. & Bozkurt, S.B., 2005. Forecasting the evolution of seismicity in southern California: animations built on earthquake stress transfer, *J. geophys. Res.*, **110,** B05S16, doi:10.1029/2004JB003475.

Vernant, P. *et al.*, 2004. Present-day crustal deformation and plate kinematics in the Middle East constrained by GPS measurements in Iran and northern Oman, *Geophys. J. Int.*, **157,** 381–398.

Waldhauser, F. & Ellsworth, W.L., 2002. Fault structure and mechanics of the Hayward Fault, California, from double-difference earthquake locations, *J. geophys. Res.*, **107,** 2054, doi:10.1029/2000JB00084.

Walker, R., 2003. Active Faulting and Tectonics of Eastern Iran, *PhD thesis*, University of Cambridge.

Walker, R.T., Andalibi, M.J., Gheitanchi, M.R., Jackson, J.A., Karegar, S. & Priestley, K., 2005. Seismological and field observations from the 1990 November 6 Furg (Hormozgan) earthquake: a rare case of surface rupture in the Zagros mountains of Iran, *Geophys. J. Int.*, **163,** 567–579.

Walpersdorf, A. *et al.*, 2006. Difference in the GPS deformation pattern of North and Central Zagros (Iran), *Geophys. J. Int.*, **167,** 1077–1088.

Yamini-Fard, F., Hatzfeld, D., Tatar, M. & Mokhtari, M., 2006. Microearthquake seismicity at the intersection between the Kazerun fault and the Main Recent Fault (Zagros, Iran), *Geophys. J. Int.*, **166,** 186–196.

Yamini-Fard, F., Hatzfeld, D., Farahbod, A.M., Paul, A. & Mokhtari, M., 2007. The diffuse transition between the Zagros continental collision and the Makran oceanic subduction (Iran): microearthquake seismicity and crustal structure, *Geophys. J. Int.*, **170,** 182–194.

Zwick, P., McCaffrey, R. & Abers, G., 1994. *MT5 Program*, IASPEI Software Library, 4.

SUPPORTING INFORMATION

Additional Supporting Information may be found in the online version of this article:

Supplement. Coulomb stress modelling at Qeshm Island.

Please note: Wiley-Blackwell are not responsible for the content or functionality of any supporting materials supplied by the authors. Any queries (other than missing material) should be directed to the corresponding author for the article.